Volume Shrinkage in Slant Fringe Gratings of a Cationic Ring-Opening Holographic Recording Material

D. A. Waldman*, H.-Y. S. Li, and M. G. Horner

Polaroid Corporation ,750M-5C, Cambridge, Massachusetts 02139

A new photopolymer holographic recording material, ULSH-500, based on cationic ring-opening polymerization, has been further optimized to achieve low transverse shrinkage without sacrificing sensitivity. The extent of transverse (z) and lateral (x) shrinkage was determined explicitly in this study for a range of slant angles in volume holograms recorded to near saturation and in holograms of low diffraction efficiency. The values $\Delta K_x/K_x$ and $\Delta K_z/K_z$, which represent the physical material shrinkage in the grating vector plane, were ascertained by (1) direct measurement of the differential angle changes in the reference and signal beam angles necessary to achieve Bragg matching and (2) measurement of the average refractive index. The accuracy of this method was primarily limited by the exactness in determining the angle of peak efficiency in the Bragg selectivity curve. It is demonstrated that the peak angle can be established to within a small fraction of a degree. It is shown that the assumption of anchoring and, thus, uniaxial shrinkage as embodied in the conventional fringe rotation model cannot be applied for the photopolymer ULSH-500 under the recording conditions used herein. It is demonstrated that background uplift in angular selectivity profiles can be attributed to nonuniformity in the grating strength throughout the transverse direction of the recording media, and that the uplift can be reduced to negligible levels by using a low fluence preimaging exposure. Calorimetric analysis of reaction kinetics was performed using direct laser irradiation delivered by optical fiber.

Journal of Imaging Science and Technology 41: 497–514 (1997)

Introduction

A photopolymer holographic recording material, ULSH-500, based on cationic ring-opening polymerization (CROP) was recently developed at Polaroid Corporation.[1] Sensitivities greater than 0.06 cm^2/mJ and refractive index modulations greater than 7×10^{-3} are achievable. Good Bragg selectivity consistent with the imaged thickness is observed, and both the angular response and the diffraction efficiency are stable in these materials without the need for post-imaging fixing procedures. Variable coating thicknesses, from 12 to at least 250 μm, have been attained. Certain limitations of conventional holographic photopolymers, such as time-consuming post-exposure fixing, oxygen sensitivity, reciprocity failure, and shrinkage, which result from the free radical chemistry typically employed, are overcome. In particular, conventional free radical polymerization produces significant volume contraction[2] which causes large angular deviations in the Bragg profile[3] and can distort the recorded fringe pattern.[4]

Volume phase holograms of digital data arranged in pages, recorded using a transparency[5] or addressable spatial light modulator,[6] optionally in conjunction with a randomized phase mask,[7,8] consist of a range of grating slant angles, each of which is formed from interference of the distinct spatial frequency components of the signal beam with the reference beam. Encoding schemes such as paraphase coding,[8] data coding based on a randomized arrangement of binary digits,[9] and representation of data in Hamming,[10] Reed-Solomon,[11] and channel codes,[12] increase the reliability of volume holographic data storage by minimizing the effect of nonuniformities in diffraction efficiency. Although error correction codes reduce the impact of various noise contributions, a tradeoff in storage capacity is inherent. Accordingly, in organic holographic recording materials it is important to diminish physical material contributions to noise such as those arising from volume shrinkage. The slant angles of volume phase gratings recorded in photopolymers are altered by anisotropic volume shrinkage attributed to densification concurrent with photopolymerization reactions. Shrinkage causes angular deviations in the Bragg profile that can exceed the angular bandwidth even for moderate slant angles. Image reconstruction (readout) of a single image, which comprises multiple gratings, is therefore likely to result in lack of image fidelity and/or distortion unless the shrinkage is reduced to extremely low levels. It is, thus, important to gain an understanding of the magnitude of shrinkage that occurs in Polaroid's CROP photopolymer holographic recording material during volume hologram formation as a function of increasing slant angle.

A derivation of the theoretical relationship between the angular shifts from the Bragg matching condition, which are measurable, and the material shrinkage in the transverse (z) and lateral (x) directions is presented here without the assumption of surface anchoring. Experiments were carried out for a range of internal slant angles between 5° and 30° to elucidate the magnitude of the respective angular deviations relative to the angular bandwidth. Accordingly, the extent of transverse and lateral shrinkage is determined explicitly for a range of slant angles and imaging conditions. Specifically, the angular responses of volume holograms recorded to near saturation as well as those

Original manuscript received April 7th, 1997.

* Corresponding author.

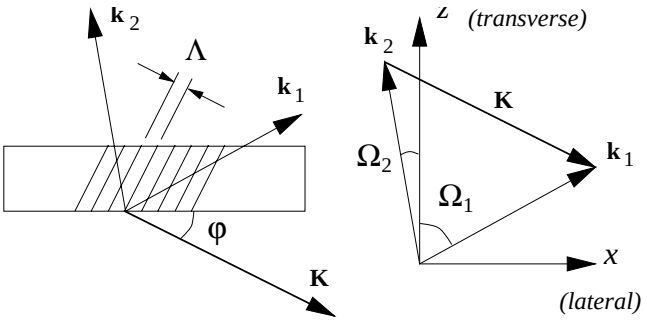

Figure 1. Schematic of grating vector components, k_1 and k_2, in the xz plane for internal signal and reference beam angles, Ω_1 and Ω_2, respectively, where ϕ is the internal slant angle and the isophase fringe planes are separated by the periodic distance, Λ.

recorded to low diffraction efficiency (on the order of 0.1 to 1%) were evaluated. Angle multiplexing schemes typically require[6b] holograms with diffraction efficiency less than about 0.1%, and which exhibit both good angular selectivity and image quality. It is shown that both properties can be achieved with a concomitant reduction in material shrinkage by utilizing a modest pre-imaging exposure. In addition, background uplift, reported on earlier[1] and attributed to nonuniformity in the grating strength recorded throughout the thickness of the material,[13] is substantially reduced to levels less than about 0.05%.

Theory

The grating vector **K** can be expressed in terms of the internal signal and reference write beam angles, $\Omega_{1_{int}}$ and $\Omega_{2_{int}}$, respectively (see Fig. 1); the average refractive index, n, of the recording medium; and the recording wavelength, λ, in vacuum as

$$\mathbf{K} = \mathbf{k}_1 - \mathbf{k}_2 = \left(K_{x,i}, 0, K_{z,i}\right) = \frac{2\pi n}{\lambda}\left(\sin\Omega_{1_{int}} + \sin\Omega_{2_{int}}, 0, \cos\Omega_{1_{int}} - \cos\Omega_{2_{int}}\right) \quad (1)$$

where i represents the initial conditions of the recording geometry.

The grating vector components along the transverse (z axis) and lateral directions (x axis), $K_{z,i}$ and $K_{x,i}$, respectively, at the initial state of recording, can be expressed in terms of the external write beam angles, $\Omega_{1_{ext}}$ and $\Omega_{2_{ext}}$, as

$$K_{z,i} = \frac{2\pi}{\lambda}\left(\sqrt{n^2 - \sin^2\Omega_{1_{ext}}} - \sqrt{n^2 - \sin^2\Omega_{2_{ext}}}\right), \quad (2)$$

$$K_{x,i} = \frac{2\pi}{\lambda}\left(\sin\Omega_{1_{ext}} + \sin\Omega_{2_{ext}}\right), \quad (3)$$

where, as shown in Fig. 1, the isophase fringe planes separated by the periodic distance, Λ, are perpendicular to the xz plane, **K** is in the xz plane normal to the isophase planes, and the external write beam angles, Ω_1 and Ω_2, are shown schematically in Fig. 2 for a general recording geometry utilized to write slant fringe plane-wave transmission holograms. A cross-sectional view of the corresponding **K**-sphere at the onset of recording is also depicted in Fig. 2.

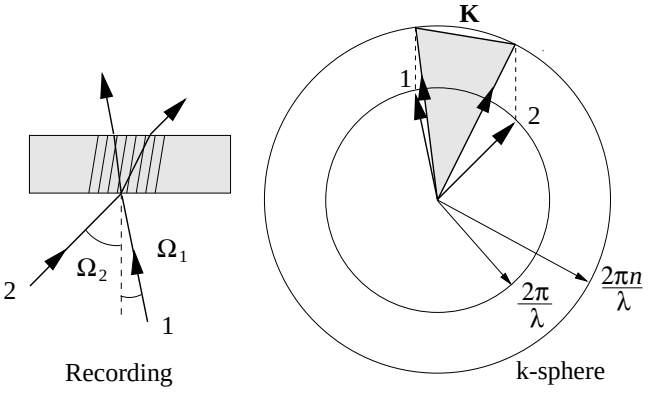

Figure 2. Schematic of general recording geometry utilized to write slant finge plane-wave transmission holograms where Ω_1 and Ω_2 are the external signal and reference write beam angles, respectively (left), and a cross-sectional view of the corresponding K-sphere, at the onset of recording, where n is the index of refraction of the medium (right).

It thus follows that the incremental changes in the grating vector components along the transverse and lateral directions, ΔK_z and ΔK_x, respectively, that arise due to shrinkage, can be expressed in terms of measurables, $\Omega_{1_{ext}}$ and $\Omega_{2_{ext}}$, and the respective angular deviations from the Bragg matching condition of the two write beams, $\Delta\Omega_{1_{ext}}$ and $\Delta\Omega_{2_{ext}}$, as

$$\Delta K_z = \frac{2\pi}{\lambda}\left(\frac{\sin\Omega_{2_{ext}} + \cos\Omega_{2_{ext}}}{\sqrt{n^2 - \sin^2\Omega_{2_{ext}}}}\Delta\Omega_{2_{ext}} - \frac{\sin\Omega_{1_{ext}} + \cos\Omega_{1_{ext}}}{\sqrt{n^2 - \sin^2\Omega_{1_{ext}}}}\Delta\Omega_{1_{ext}}\right) + \frac{2\pi}{\lambda}\left(\frac{\Delta n}{n}\right)\left(\frac{n^2}{\sqrt{n^2 - \sin^2\Omega_{1_{ext}}}} - \frac{n^2}{\sqrt{n^2 - \sin^2\Omega_{2_{ext}}}}\right) \quad (4)$$

and

$$\Delta K_x = \frac{2\pi}{\lambda}\left(\cos\Omega_{1_{ext}}\Delta\Omega_{1_{ext}} + \cos\Omega_{2_{ext}}\Delta\Omega_{2_{ext}}\right) \quad (5)$$

where Δn is the change in refractive index that occurs during recording. Figure 3 illustrates the resultant changes in the Bragg matching representation in **K**-space in cross-sectional view due to anisotropic volume shrinkage and an accompanying increase in refractive index (i.e., expansion of sphere and rotation of the grating vector).

The change in internal slant angle, $\Delta\phi$, can be expressed in terms of the initial lateral and transverse grating components, $K_{x,i}$ and $K_{z,i}$, and the respective changes, ΔK_x and ΔK_z, as

$$\Delta\phi_{slant} = \frac{\left(K_{x,i}\Delta K_z - K_{z,i}\Delta K_x\right)}{{K_{x,i}}^2 + {K_{z,i}}^2} \quad (6)$$

where during shrinkage the grating period component, Λ_x, is not assumed to be fixed as the grating slant angle rotates to an increased angle, contrary to the boundary conditions of the fringe rotation model. The relative changes in the transverse (perpendicular to the film plane) and lateral (parallel to the film plane) components of the grat-

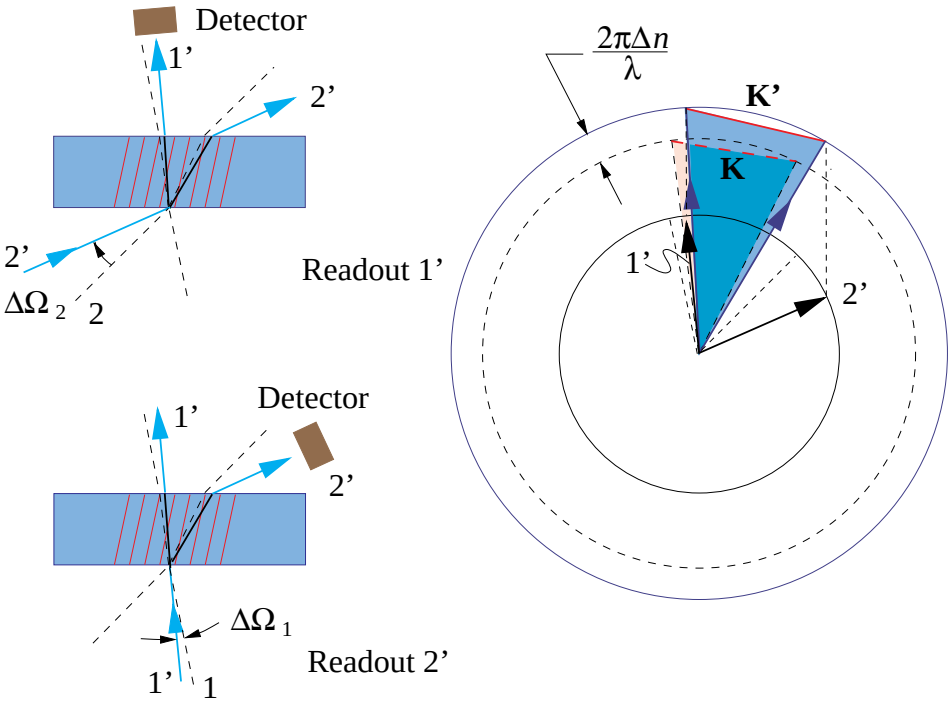

Figure 3. Schematic of readout method utilized to measure external angular deviations from Bragg matching condition, $\Delta\Omega_1$ and $\Delta\Omega_2$, for slant fringe plane-wave transmission holograms (left), and illustration of resultant changes in the Bragg matching representation in **K**-space, in cross-sectional view (right) due to anisotropic volume shrinkage and accompanying increase in refractive index (i.e., expansion of sphere and rotation of the grating vector).

ing vector, $-\Delta K_z/K_{z,i}$ and $-\Delta K_x/K_{x,i}$, respectively, are equal to the physical material shrinkage along the respective directions independent of slant angle ϕ. Referring to Fig. 1 and assuming uniaxial shrinkage, the grating periods in the transverse direction, Λ_z, before and after recording are

$$\Lambda_{z,i} = \frac{\Lambda_i}{\cos\phi_i} \tag{7}$$

$$\Lambda_{z,f} = \frac{\Lambda_i}{\cos\phi_f} \tag{8}$$

where $K_z = 2\pi/\Lambda_z$ and $\Delta K_z/K_z = -\Delta\Lambda_z/\Lambda_z$. Generally, regardless of whether the shrinkage is uniaxial, $\Delta K_x/K_x = -\Delta\Lambda_x/\Lambda_x$. Clearly, $\Delta K/K_i$ varies depending on the slant angle, but although the magnitude $\Delta K/K_i$ directly represents the amount of dimensional change along the grating vector direction, it does not provide directional information and contains no contribution from the lateral y direction. To assess the relative volume change, $\Delta V/V$, during recording requires an assumption of homogeneity in the lateral directions (i.e., $\Delta x/x = \Delta y/y$), which is reasonable for volume hologram formation in photopolymers considering that the final recorded state is a glassy material. The relative volume shrinkage can thus be expressed as

$$\frac{\Delta V}{V} = -\left(\frac{\Delta K_z}{K_{z,i}} + \frac{2\Delta K_x}{K_{x,i}}\right). \tag{9}$$

Experimental

Materials. ***Photoacid Generators.*** The photoacid initiator, 4-octyloxyphenyl(phenyl)iodonium hexafluoroantimonate, (OCTO), was prepared following the procedure of Crivello and Lee.[14] Octylphenyl ether was coupled with hydroxy(tosyloxy)iodobenzene to yield 4-octyloxyphenyl(phenyl)iodonium tosylate. Metathesis of the tosylate with sodium hexafluoroantimonate followed by recrystallization yielded the desired antimonate salt as a white crystalline solid. Octylphenyl ether was prepared by alkylating phenol with 1-bromooctane in acetonitrile using K_2CO_3 (anh) and a phase transfer catalyst, crown ether 18-crown-6. The product was purified by vacuum distillation. All other materials were purchased from Aldrich Chemical Company and used as received. Bis (methylphenyl)iodonium tetrakis(pentafluoro-phenyl) borate (MPIB) was obtained from Rhone Poulenc as Silcolease UV Cata Poudre™ 200 and was purified by recrystallization from methylene chloride:hexane or 2-propanol:water, and dried before use.

Dye Sensitizer. 5,12-bis(phenylethynyl)naphthacene (BPEN) was purchased from Aldrich Chemical Company and used as received.

Monomers. All monomers have two or more cyclohexene oxide (CHO) groups linked through siloxane chain segments. The difunctional monomer, 1,3-bis[2-(3{7-oxabicyclo [4.1.0]heptyl})ethyl]-tetramethyl disiloxane (DiEPOX), was obtained as an experimental chemical from General Electric Corporation and was distilled under vacuum before use. Monomers with more than two polymerizable CHO groups were synthesized by hydrosilylation of vinylcyclohexene oxide with a methylhydrosiloxane molecule, as reported ealier.[1] Specifically, a multifunctional monomer with four polymerizable CHO groups, 3,3-bis[[dimethyl[2-(7oxabicyclo[4.1.0]hept-3-yl)ethyl]silyl]oxy]-1,1,5,5-tetramethyl-1, 5-bis[2-(7-oxabicyclo[4.1.0]hept-3-yl)ethyl] trisiloxane was synthesized by hydrosilylation of tetrakis-(dimethylsiloxy)silane with 4-vinyl-1-cyclohexene 1,2-epoxide using $Rh(PPh_3)_3Cl$ as a catalyst. Isolation of the compound from the reaction mixture was accomplished by treatment with activated charcoal, filtration through a pad of Celite™, and removal of solvent in vacuo. Purification was carried out by dissolving in hexane and treating twice with activated charcoal, each followed by filtration, or by dissolving in methylene chloride and effecting chromatography on silica gel with methylene chloride:acetone as an eluent.

Binders. Poly(methylphenylsiloxane), 710™ fluid, viscosity 500 centistokes, DOW Corning, was purchased from

Aldrich; 1,3,5-trimethyl-1,1,3,5,5-pentaphenyltrisiloxane, 705™ fluid, DOW Corning, was obtained from DOW Corning.

Sample Preparation. Formulations were made by mixing photoacid generator, 4 to 10% (w/w), sensitizing dye, 0.03 to 0.1% (w/w), monomer(s), 40 to 75% (w/w), and binder, 20 to 60% (w/w). The resulting clear viscous fluid was purged with argon for at least 12 h to remove solvent and then spread by capillary action between two glass plates separated by a polytetraflouroethylene spacer of known thickness. Edges of the cells were sealed with low-temperature hot-melt polyethylene to prevent incursion of moisture.

Holographic Exposure. Unslanted plane-wave transmission holograms were recorded in the conventional manner with two spatially filtered and collimated argon ion laser writing beams at 514.5 nm with equal irradiance levels directed onto the sample with equal semiangles of 25° about the normal. Slant fringe plane-wave transmission holograms were recorded with a frequency doubled Nd:YAG laser at 532 nm using two spatially filtered and collimated laser writing beams directed onto the sample with an interbeam angle of either 32°0' or 34°10'. The intensities of the two beams were adjusted to compensate for relative angle cosine factors. The sample was mounted onto a motorized rotation stage, model 495 from Newport Corporation. The rotational position of the stage and, thus, the angle of the sample plane relative to the writing beams was computer controlled via a motion controller, model PMC200P from Newport Corporation. Accordingly, for the holographic exposures reported herein the interbeam angle of the signal and reference beam paths remained fixed, while the sample recording material was rotated to alter the grating angle of the resultant slant fringe hologram. The formulations described in this study were not sensitive to red light, hence a beam expanded HeNe probe beam, incident at the appropriate Bragg angle, was used to detect the development of holographic activity during exposure. Real-time diffraction intensity data were obtained using two model 818-SL photodiodes and a dual-channel multifunction optical meter, model 2835-C from Newport Corporation.

Nonholographic Pre-Imaging Exposure. Pre-imaging exposure was carried out with one spatially filtered and collimated argon ion laser writing beam at 514.5 nm, directed onto the recording medium at about normal incidence while the sample was vibrated. The exposure irradiance was kept constant at about 0.4 mW/cm^2 and the time of exposure was varied to provide a range of fluence between 5 and 40 mJ/cm^2. A reduction in absorbance of the recording medium and an increase in the viscosity of the recording medium resulted.

Angular Selectivity. Angular selectivity measurements were performed using spatially filtered and collimated laser reading beams from a frequency doubled Nd:YAG laser at 532 nm with incident power of about 20 μW. The sample was mounted on a motorized rotation stage, as during recording, and thus the angle of the sample plane relative to either the reference or signal beam was computer controlled via a motion controller, model PMC200P from Newport Corporation. The read angle was detuned from the recording state while maintaining the sample in its original mount position, and the diffraction efficiency was measured at each angular increment with photodiodes and an optical meter from Newport Corporation (see above). The angular resolution was 0.001° and the experimentally determined repeatability was ≤ 0.005°, which was attained by use of unidirectional rotation during measurement thereby eliminating any effect from backlash of the compliant worm gear. Accordingly, for the measurements reported herein the signal and reference beam paths remained fixed with an interbeam angle of either 32°0' or 34°10', while the surface plane of the volume hologram was rotated to alter the incident angle of the signal and reference readbeam paths. Measurement of angular selectivity was carried out independently for the signal and reference beams, as illustrated in Fig. 3 along beam paths 1-2' (Readout 2') and 2-1' (Readout 1'), respectively, by rotation of the hologram over a range of plus/minus several degrees from the recording position at increments of $0.001° \leq \Delta\theta \leq 0.02°$. In this manner, during reconstruction of the volume hologram, angular deviations from the recording condition necessary to achieve Bragg matching, $\Delta\Omega_1$ and $\Delta\Omega_2$, were obtained explicitly for the signal and reference beams for each slant fringe construction.

Refractive Index. Refractive index measurements were carried out using a Bausch & Lomb temperature controlled refractometer. The accuracy of this measurement was estimated to be about $\pm 2 \times 10^{-4}$. The measured values, n_d, and dispersion, K, were utilized to calculate values of refractive index at the read wavelength, 532 nm, and are reported as such. Coatings of 135 μm thickness were prepared using rectangular substrates of SF 56 crystal (n_d = 1.78557) and polytetraflouroethylene spacers. Measurements were carried out in a fully darkened room on non-exposed fluid coatings, representing the initial state, on coatings exposed (argon ion laser at 514 nm) to varying amounts of pre-imaging fluence, and on coatings exposed to saturation.

Differential Scanning Photocalorimetry. Cationic ring-opening polymerization is an exothermic process, and polymerization rates and extents of monomer conversion can, therefore, be determined through calorimetry. Calorimetric analysis was performed on a Perkin-Elmer DSC-7 differential scanning calorimeter equipped with a DPC-7 photocalorimeter module. Samples, 1.0 to 3.0 mg, were irradiated in the calorimeter with the 514.5-nm line from a Spectra-Physics 161C-514 laser at intensities between 0.1 and 10 mW/cm^2, utilizing a multimode (200-μm core) fiber optic cable. Samples were equilibrated at 30°C for 1 to 4 min prior to illumination. The heat flow required to maintain the sample at a constant temperature (30°C) was recorded at time intervals of 0.40 seconds. This data was integrated to determine the evolved heat of reaction versus illumination time, which after appropriate normalization was converted to the extent of reaction versus time. Data were first corrected to remove sources of extraneous heat flow. The corrected heat flow curve was then analyzed using the rectangular formula for definite integrals without any smoothing over time slices of 0.67 seconds. The fractional extent of reaction as a function of time, $\phi(t)$, was then determined from the relation

$$\phi(t) = \sum_{t=0}^{t} \frac{q(t)}{\Delta H_{rxn}}, \tag{10}$$

where $q(t)$ is the heat evolved after illumination time t and ΔH_{rxn}, the heat of light-induced reaction, is taken as the area under the complete corrected heat flow curve.

Small sample weights were used to minimize effects due to sample thickness and thermal transfer.

Results and Discussion

Dual Differential Angle Measurement Method. In the original form of the fringe-plane rotation (FPR) model, substrate anchoring was assumed, and the thickness ratio in the transverse direction, t'/t, where t' is the final thickness of the hologram, was approximated[15] as the ratio of initial to final slant angles, ϕ/ϕ'. Although measurements of both signal and reference beams angles were used to determine the respective slant angles, the approximation error for moderate slant angles is significant, especially if shrinkage levels are low. For photopolymers the approximation was compounded further by not considering changes in the refractive index. The typical method used to assess the amount of shrinkage during hologram formation in photopolymers, however, only comprised determining the value of $\Delta\Omega_{2_{ext}}$ necessary to achieve maximum reconstruction diffraction efficiency.[3] This is described in a more recent form of the FPR model where the grating slant angle after shrinkage is given by

$$\phi' = \phi + \Delta\phi = \tan^{-1}\left[\frac{\tan\phi}{1-\alpha}\right], \tag{11}$$

where α is the coefficient of shrinkage and $\Delta\phi$ is equated[16] with $\Delta\Omega_{2_{ext}}$. Accordingly, this FPR model approximates the resultant increase in grating slant angle of the recorded hologram and consequently also approximates the coefficient of shrinkage. Moreover, the volume change deduced by Eq. 11 is not determined from the reduction in grating period, and implicitly it is assumed that no dimensional change occurs in the lateral directions due to anchoring at the substrate interface. The internal slant angle after shrinkage can be expressed in terms of the two differential angles, $\Delta\Omega_{1_{ext}}$ and $\Delta\Omega_{2_{ext}}$, (using notation in the above theory section) and the refractive index change, Δn, as

$$\phi' = 0.5\left\{\sin^{-1}\left[\frac{\sin\left(\Omega_{2_{ext}} + \Delta\Omega_{2_{ext}}\right)}{n+\Delta n}\right] - \sin^{-1}\left[\frac{\sin\left(\Omega_{1_{ext}} + \Delta\Omega_{1_{ext}}\right)}{n+\Delta n}\right]\right\} \tag{12}$$

If the assumption of anchoring is made, then determining $\Delta\Omega_{2_{ext}}$ also defines $\Delta\Omega_{1_{ext}}$ (from Eq. 5 with $\Delta K_x = 0$), and thus the grating period and coefficient of shrinkage can be ascertained under the defined boundary conditions (i.e., rotation occurs in the xz plane), as in Eq. 22 of Ref. 16.

The assumption of anchoring, however, is not made in the Dual Differential Angle Measurement (DDAM) model presented here, and additionally the proposed model provides sufficient information by measurement of both $\Delta\Omega_{1_{ext}}$ and $\Delta\Omega_{2_{ext}}$ so that the effect on grating period is manifested. The magnitude of dimensional change in the grating period along the x and z directions, $-\Delta K_x/K_{x,i}$ and $-\Delta K_z/K_{z,i}$, that occurs during hologram formation was calculated explicitly from the shift in the grating vector components using Eqs. 4, 5, 7, and 8 by (1) measuring the deviation of the Bragg angle from the external reference and signal beam write angles and (2) determining the change in the average refractive index of the holographic recording medium. The former was obtained by directly measuring the differential angle changes in the reference and signal beam angles, necessary to achieve Bragg matching, by rotation of the sample (i.e., the recording geometry is not altered). The latter was measured to within 2×10^{-4} using a Bausch & Lomb refractometer. Since the bond order does not change during CROP polymerization, hence the increase in refractive index that results during exposure of the recording medium is due predominantly to densification of the material. The readout method for $\Delta\Omega_{2_{ext}}$ and $\Delta\Omega_{1_{ext}}$ is depicted schematically in Fig. 3 by Readout 1' and Readout 2', respectively.

The initial angular position of the sample plane at the time of imaging, and thus the recording slant angle, was determined by first using back reflections from a HeNe laser through apertures of 1 mm to set the zero degree or normal incidence condition and then rotating the sample plane to the desired recording state. The error associated with determining the initial slant angle, based on repeatability of measuring both the normal incidence condition ($\leq 0.003°$) and the starting refractive index (± 0.0002), is estimated to be $\leq 0.0045°$ for $\phi = 20°$. The error in defining the recording slant angle, however, does not impact measurement of the differential external angles, $\Delta\Omega_{1_{ext}}$ and $\Delta\Omega_{2_{ext}}$, as these were measured directly by use of an optically encoded rotation stage. The position of the sample in its holder is unaltered from the onset of imaging to readout. Consequently, the accuracy of this method (i.e., direct measurement of differential angles) is primarily limited by the exactness in determining the angle of maximum diffracted intensity in the Bragg selectivity curve. For a typical angular scan, the experimental method described here can be utilized to establish the peak angle to within a small fraction of a degree (e.g., $\pm 0.01°$). Accordingly, this method allows one to ascertain both ΔK_x and ΔK_z, and thereby directly determine values for transverse and lateral shrinkage in the plane of the grating vector, **K**.

Shrinkage in Slant Fringe Holograms Recorded to Near Saturation. ***Angular Shifts.*** Results are presented in Tables I and II and Figs. 4 and 5 for slant fringe plane-wave holograms recorded to near saturation in the CROP photopolymer. In Fig. 4 values of $\Delta\Omega_{1_{ext}}$ and $\Delta\Omega_{2_{ext}}$ are plotted versus grating slant angle, f, for individual holograms recorded with f between about 0.03° and 30°. The magnitude of the angular deviations reported here are about one fifth that reported recently for a slant fringe hologram recorded with similar grating angle in a conventional photopolymer based on radical chemistry.[3] Results for the CROP photopolymer are shown both immediately after recording and after a wait time of 24 hours under dark storage conditions, during which the angle deviations shifted additionally by small amounts and then stabilized at plateau values. The magnitude of the deviation from the recording Bragg matching condition typically increased during dark storage over a period of 2 to 3 hours from the onset of recording, indicating that further polymerization occurred due to the living nature of cationic polymerizations. The full dynamic range of the recording medium was deliberately not consumed during imaging as a preventive measure to ensure that holograms formed in coatings of these thicknesses (greater than 50 μm) did not become overmodulated. A post-imaging flood exposure at the recording wavelength can, however, be implemented to consume the remaining dynamic range of the photopolymer, thereby causing the full shift to occur immediately.

The results displayed in Fig. 4 confirm that volume holograms recorded with larger grating slant angles exhibit a concomitant increase in their respective angular shifts from the Bragg matching condition. This increase is con-

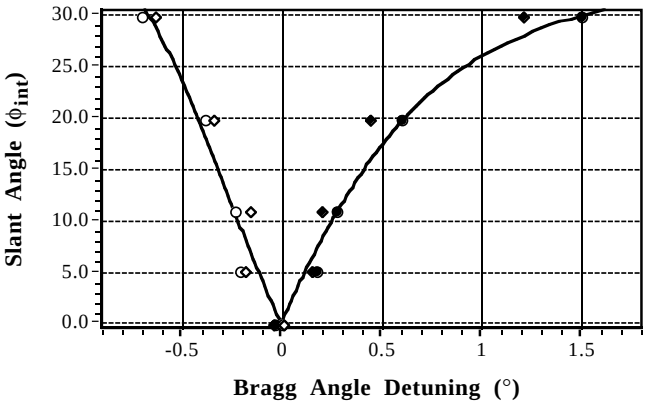

Figure 4. Plot showing angular deviations from Bragg matching condition, $\Delta\Omega_{1_{ext}}$ and $\Delta\Omega_{2_{ext}}$, as a function of internal slant angle, ϕ, for slant fringe plane-wave volume holograms recorded to near saturation in the CROP photopolymer, where $\Delta\Omega_{1_{ext}}$ (◇) and $\Delta\Omega_{2_{ext}}$ (◆) were obtained immediately after recording, and $\Delta\Omega_{1_{ext}}$ (○) and $\Delta\Omega_{2_{ext}}$ (●) were obtained after a wait time of 24 hours under dark storage conditions followed by a flood exposure of about 45 mJ/cm^2. The solid lines represent numerical results, according to the fringe-plane rotation model, where Δn is considered and anchoring at the substrate interface in the lateral directions is assumed (see text).

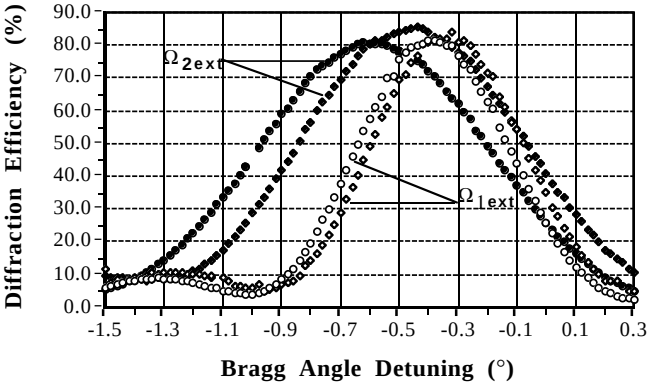

Figure 5. Angle selectivity profiles showing angular deviations, $\Delta\Omega_{1_{ext}}$ and $\Delta\Omega_{2_{ext}}$, from the recording Bragg matching condition for a slant fringe hologram with internal slant angle, ϕ, of 20° (◇), (◆) obtained immediately after recording, and (○), (●) obtained after a wait time of 24 h under dark storage conditions followed by a flood exposure of about 45 mJ/cm^2. Resolution of angle data collection was 0.001° and increment plotted is 0.02°.

sistent with contributions to physical shrinkage that arise from the relation between increased slant angle and larger transverse components of the grating vector, as apparent from Eq. 6. If it is assumed that the magnitude of transverse shrinkage is constant for all slant angles, then a comparison can be readily made with the fringe plane rotation model. Numerical results according to the fringe rotation model, but with the inclusion of refractive index change, are shown in Fig. 4 (solid lines) for the range of grating slant angles studied. The parameters chosen were consistent with (1) the recording geometry (i.e., fixed interbeam angle, $\Omega_{ib} = 34.05°$); (2) the material properties used for calculations in Tables I and II and described below, namely $n = 1.5206$ and $\Delta n = 0.0099$; and (3) a transverse shrinkage of $-\Delta K_z/K_{z,i} = 0.8\%$, which as shown below corresponds to that determined from the differential angle method at slant angles of $\phi > 5°$. Evidently, the angular shifts observed for slant fringe plane-wave holograms recorded to near saturation exhibit dependence on grating slant angle similar to that predicted by a fringe rotation model when the model is modified such that both angular deviations and the refractive index change are incorporated. The magnitude of the relative differences in angular shifts as a function of grating slant angle is an important performance criterion in considering holographic materials for applications such as optical data storage. For example, if the differences are large for a single image that comprises multiple gratings, such as for a Fourier image, then image reconstruction will display lack of image fidelity and consequently distortion, thereby impairing the achievable raw error bit rate.

Counterclockwise rotations of the sample plane, for slant fringe holograms with internal grating angles of $\phi \geq 5°$, were required to Bragg match $\Omega_{1_{ext}}$ and $\Omega_{2_{ext}}$ immediately after recording. The differential angle changes, $\Delta\Omega_{1_{ext}}$ and $\Delta\Omega_{2_{ext}}$, were thus negative (–) and positive (+), respectively, regardless of whether the signal and reference beam recording angles were in the same or different quadrants (see Fig. 2). The requisite counterclockwise rotation increased slightly during the wait time necessary to attain stable plateau values. Accordingly, the final signs of $\Delta\Omega_{1_{ext}}$ and $\Delta\Omega_{2_{ext}}$ for $\phi \geq 5°$ were (–) and (+), respectively, which indicates that the grating slant angle increased and the grating period decreased. Modest levels of shrinkage, attributed to densification concurrent with photo-polymerization, has typically caused angular deviations in the Bragg profile that can exceed the angular bandwidth even for moderate slant angles. Examples of angular selectivity profiles for $\phi = 20°$ are shown in Fig. 5 as measured immediately after recording was finished and then after a wait time sufficient for stabilization of the angular shifts. The increased half width of the angular profile for $\Omega_{2_{ext}}$ relative to that for $\Omega_{1_{ext}}$ is due to the angle of incidence for the former being larger (i.e., for $\phi = 20°$; $\Omega_{1_{ext}} = -15°$, $\Omega_{2_{ext}} = 49.05°$).

In Table I are listed measured values of $\Omega_{1_{ext}}$, $\Omega_{2_{ext}}$, $\Delta\Omega_{1_{ext}}$, and $\Delta\Omega_{2_{ext}}$ and the corresponding internal grating slant angles at the onset of recording, ϕ_o, the initial state at which stable diffraction efficiency is first observed, ϕ_i, and the final physical state of the holographic recording medium, ϕ_f. At the onset of recording, the material is a fluid, whereas when stable grating formation first occurs the material is in a pregelatinous state, and after recording and achieving the full extent of cure, the material is in a glassy state. Accordingly, the initial value of the refractive index, used in Table I and for calculations of $\Delta K_x/K_{x,i}$ and $\Delta K_z/K_{z,i}$ listed in Table II, was ascertained from measurement of the recording medium after an imaging exposure equivalent to the requisite fluence for observation of stable diffraction efficiency (i.e., $\eta \sim 0.25\%$). The physical state of the recording medium after such an exposure comprises sufficient microstructural integrity to manifest a stable fringe structure with defined spatial frequency. This exposure exceeds the threshold exposure fluence, defined here as the fluence necessary to detect holographic activity, by a few mJ/cm^2. For purposes of calculating the physical material shrinkage, $\Delta V/V$, this method provides a more equitable estimate of the initial refractive index during hologram formation, when recording to near saturation, than would values at the onset of recording. Use of the former likely results in a conservative estimate of the physical material shrinkage, whereas employing the latter could effect a consequential underestimate of $\Delta K_z/K_{z,i}$ ($\Delta K_x/K_{x,i}$ is independent of Δn), if a significant change in refractive index occurs during early stages of hologram

TABLE I. External Angles Used for Recording Plane-Wave Slant Fringe Holograms to Near Saturation, Calculated Internal Grating Angles, and Deviations of Recording External Angles from the Bragg Matching Condition Resulting from Volume Change that Occurs during Hologram Formation

Slant fringe holograms*	5°	10°	20°	30°
External angles and Bragg shifts				
$\Omega_{1_{ext}}$ (°)†	8.1	0.0	- 15.0	- 34.0
$\Omega_{2_{ext}}$ (°)†	23.9	34.05	49.05	68.05
$\Delta\Omega_{1_{ext}}$ (°)‡	- 0.21	- 0.23	- 0.38	- 0.70
$\Delta\Omega_{2_{ext}}$ (°)‡	+ 0.175	+ 0.28	+ 0.60	+ 1.50
Grating slant angles, ϕ				
ϕ_o (°)§	5.093	10.858	19.894	29.743
ϕ_i (°)‖	5.068	10.803	19.791	29.582
ϕ_f' (°)¶	5.156	10.886	19.922	29.793
ϕ_f (°)**	5.157	10.887	19.923	29.802

***** Slant fringe holograms were recorded to near saturation with internal slant angles, ϕ, of about 5°, 10°, 20°, and 30° (see Figs. 1 and 2 for recording geometry).

† $\Omega_{1_{ext}}$ and $\Omega_{2_{ext}}$ are external signal and reference recording angles, respectively. The external interbeam angle for $\phi \cong 5°$ was 32.0° and for $\phi \geq 10°$ was 34.05°.

‡ $\Delta\Omega_{1_{ext}}$ and $\Delta\Omega_{2_{ext}}$ are deviations of the external signal and reference beam read angles from the Bragg matching condition (see Fig. 3 and equations in text).

§ ϕ_o is internal slant angle at onset of recording where $n_{0,532} = 1.5133$ (see text).

‖ ϕ_i is internal slant angle when stable diffraction efficiency is first observed, where $n_{i,532} = 1.5206$ (see text).

¶ ϕ_f' is final internal slant angle after photopolymer is fully cured and is calculated by adding $\Delta\Omega_{1_{ext}}$ to $\Omega_{1_{ext}}$ and $\Delta\Omega_{2_{ext}}$ to $\Omega_{2_{ext}}$ and then determining the slant angle using $n_{f,532} = 1.5305$ (see Eq. 12 in text).

****** ϕ_f is final internal slant angle after photopolymer is fully cured and is calculated by taking the first order approximation of $\Delta\phi$ (as a function of $\Omega_{1_{ext}}$, $\Omega_{2_{ext}}$, $\Delta\Omega_{1_{ext}}$, $\Delta\Omega_{2_{ext}}$, and $\Delta n = n_f - n_i$) and then adding $\Delta\phi$ to ϕ (see Eq. 6 in text).

formation. The final value of the refractive index used in Tables I and II corresponds to that measured after the photopolymer recording medium was exposed with a non-holographic fluence commensurate with that needed to consume the entire dynamic range. Additionally, when the change in average refractive index is not included, as for the models in Refs. 15 and 16, then the values calculated for volume shrinkage are generally overestimated.

Grating Vector Components. In Table II calculated values of $\Delta K_x/K_x$ and $\Delta K_z/K_z$ are listed which are equal to the negative of the relative changes in grating period in the lateral and transverse directions, $-\Delta\Lambda_x/\Lambda_x$ and $-\Delta\Lambda_z/\Lambda_z$, respectively, for holograms recorded to near saturation with a range of grating slant angles between about 5° and 30°. The magnitude of the physical material shrinkage along the transverse direction, when the conservative approach is adopted, was on the order of 0.8% for internal slant angle $\phi \geq 10°$, and similarly the average volume change was about 0.8%. This is in close agreement with the increase in refractive index, $\Delta n = 0.65\%$, exhibited by the recording medium during formation of holograms with high diffraction efficiency, and is less than the total increase of 1.14% ($\Delta n_{532} = +0.0172$) between the fluid state and the fully polymerized glass state. CROP is not accompanied by a change in bond order, and thus the increase in refractive index that occurs during polymerization is directly related to densification of the recording material. For $\phi = 5°$ the magnitude of shrinkage along the transverse direction was enlarged to 1.61% whereas the volume shrinkage, 1.31%,

TABLE II. Calculated Relative Changes in the Grating Vector along the Transverse and Lateral Directions, and the Relative Material Volume Change with the Assumption of Homogeneity in the Lateral Directions, for Plane-Wave Slant Fringe Holograms Recorded to Near Saturation. Results from the Fringe Rotation Model, with and without Inclusion of Δn, and Those Obtained using Both the First-Order Approximation and Direct Solution of the DDAM Model.

Slant fringe holograms*	5°	10°	20°	30°
First order solution				
$\Delta\phi$ (°)†	0.089	0.084	0.133	0.221
$\Delta K_z/K_{z,i}$ (%)‡	1.613	0.801	0.818	0.804
$\Delta K_x/K_{x,i}$ (%)‡	- 0.153	0.006	0.092	- 0.093
$-\Delta V/V$ (%)§	1.307	0.813	1.002	0.617
Direct solution				
$\Delta\phi$ (°)‖	0.088	0.083	0.131	0.211
$\Delta K_z/K_{z,i}$ (%)¶	1.598	0.793	0.802	0.690
$\Delta K_x/K_{x,i}$ (%)¶	- 0.154	0.005	0.085	- 0.168
$-\Delta V/V$ (%)**	1.291	0.803	0.972	0.353
Fringe rotation model				
$-\Delta V/V$ (%)††	1.724	0.782	0.711	0.852
$-\Delta V/V$ (%)‡‡	2.386	1.473	1.464	1.730
$-\Delta V/V$ (%)§§	2.233	1.531	1.602	1.811

***** Slant fringe holograms were recorded to near saturation with internal slant angles, ϕ, of about 5°, 10°, 20°, and 30° (see Figs. 1 and 2 for recording geometry).

† $\Delta\phi$ determined by taking the first-order approximation (see Eq. 6 in text) where components of K and ΔK in lateral and transverse directions are defined in Eqs. 2, 3, 4, and 5, and $\Delta n = n_{f,532} - n_{i,532}$ as in Table I.

‡ $\Delta K_z/K_{z,i}$ and $\Delta K_x/K_{x,i}$ are the relative changes in the grating vector components along the transverse and lateral directions (equals the negative of the material shrinkage, $-\Delta\Lambda_z/\Lambda_z$ and $-\Delta\Lambda_x/\Lambda_x$, in the z and x directions, independent of slant angle) and are calculated using the first order approximation from Eqs. 4 and 5).

§ $-\Delta V/V$ is determined using Eq. 9 and the first order approximation for $\Delta K_z/K_{z,i}$ and $\Delta K_x/K_{x,i}$ and assuming that dimensional changes in x and y are equal.

‖ $\Delta\phi$ is determined by direct solution using Eq. 12, where measured values of angles and Bragg shifts are from Table I and $\Delta n = n_{f,532} - n_{i,532}$.

¶ $\Delta K_z/K_{z,i}$ and $\Delta K_x/K_{x,i}$ are calculated by direct solution using Eqs. 2 and 3, by adding $\Delta\Omega_{1_{ext}}$ to $\Omega_{1_{ext}}$, $\Delta\Omega_{2_{ext}}$ to $\Omega_{2_{ext}}$, and Δn to n, to obtain ΔK_z and ΔK_x.

****** $-\Delta V/V$ is calculated by direct solution using $\Delta K_z/K_{z,i}$¶ and $\Delta K_x/K_{x,i}$¶ in Eq. 9.

†† $-\Delta V/V$ is calculated by using Eq. 12 to determine the slant angle after recording, thus including the effect of Δn, and then taking the ratio of the tangents of ϕ_i and ϕ_f' as described in the method of Ref. 15.

‡‡ $-\Delta V/V$ is calculated according to the method of Ref. 15; therefore $\Delta n = 0$.

§§ $-\Delta V/V$ is calculated according to the method of Ref. 16; thus $\Delta n = 0$, $\Delta\phi = \Delta\Omega_{2_{ext}}$.

was slightly lower than the transverse value due to a small positive dimensional change in the lateral direction. An increase of only +0.025° and +0.015° for the measured values of $\Delta\Omega_{1_{ext}}$ and $\Delta\Omega_{2_{ext}}$, respectively, which is slightly larger than the predicted accuracy of ±0.01° (based on angular resolution and smooth peak shape), would reduce the calculated value of $\Delta\Lambda_x/\Lambda_x$ to essentially zero and increase the value of $\Delta\Lambda_z/\Lambda_z$ slightly to 1.67%. The 1 cm^2 imaged area was, however, surrounded by the remaining fluid recording medium, and thus it is possible that fluid permeated the crosslinked microstructure of the hologram and thereby effected a slight swelling of the shrinkage state. The magnitude of $\Delta\Lambda_x$ is close to zero, and consequently a slight swelling in the lateral direction would be manifested as an overall expansion of Λ_x, whereas the magnitude of $\Delta\Lambda_z$ is about 10 times greater and thus largely unaffected.

The changes in internal slant angle are also listed in Table II where the values were determined by using the

aforementioned methods for measuring differential angle changes and refractive indices. The increases in grating slant angle occurring during hologram formation were small, and although the magnitude increased in monotonic fashion with larger slant angles for $\phi > 5°$, the percentage change was less than 1%. Near unslanted plane-wave holograms (e.g., $\phi = -0.03°$) exhibited extremely small angular deviations, $\Delta\Omega_{1_{ext}} = -0.03°$ and $\Delta\Omega_{2_{ext}} = 0.003°$, from the Bragg matching condition, indicating that negligible dimensional change occurred along the lateral direction under these recording conditions. The error associated with determining the physical volume change from relative changes in the components of the grating vector is, however, quite large for cases where the slant angle is less than about 3°. At small slant angles the values of $K_{z,i}$, which are fractional and about a factor of 10 smaller than ϕ, dominate determination of $\Delta K_z/K_{z,i}$. Consequently, even small errors in ϕ, and thus $\Omega_{1_{ext}}$ and $\Omega_{2_{ext}}$, have a significant effect on the magnitude of $\Delta K_z/K_{z,i}$, as apparent from Eqs. 4 and 5. Experimental errors in $\Delta\Omega_{1_{ext}}$ and $\Delta\Omega_{2_{ext}}$ are thus amplified for small grating slant angles and in such cases contribute to large uncertainties in the final calculated value of the change in physical volume.

Values of $\Delta K_x/K_{x,i}$, $\Delta K_z/K_{z,i}$, and $\Delta V/V$ were determined by using Eqs. 2 and 3 for an exact solution by adding $\Delta\Omega_{1_{ext}}$ to $\Omega_{1_{ext}}$, $\Delta\Omega_{2_{ext}}$ to $\Omega_{2_{ext}}$, and Δn to n, to obtain K_x and K_z after recording (Table II). Results from the first-order approximation, obtained using Eqs. 4 and 5, agree closely with results of the exact solution for holograms recorded with grating slant angles of ≤20°. The first-order approximation, however, effects an overestimate for the magnitude of shrinkage along the transverse direction when the internal grating slant angle $\phi \cong 30°$. Although the shrinkage is low, the size of the Bragg mismatch for $\phi \cong 30°$ is sufficiently large to cause the difference noted. Results displayed in Fig. 4 and listed in Tables I and II establish that volume holograms recorded with increasingly larger grating slant angles, and that undergo essentially equal amounts of shrinkage in the transverse direction during hologram formation exhibit a concomitant increase in their respective angular shifts from the Bragg matching condition. Accordingly, if the amount of shrinkage is small, as for the ULSH-500 photopolymer recording medium, then the first-order approximation of DDAM provides a satisfactory method for determining shrinkage, except for cases involving large grating slant angles where the Bragg mismatch may be large. Conversely, if the amount of shrinkage is moderate (i.e., several percent or larger) then the magnitude of the Bragg mismatch is necessarily large, even for small grating angles,[3] and thus the exact solution of the DDAM method should be applied, except over a narrow range of small grating angles. Moreover, as shown in Table II, the degree of overestimation for the extent of shrinkage increases significantly when the conventional fringe rotation model is used (i.e., the change in refractive index is not considered and $\Delta\Lambda_x = 0$). When the fringe rotation model is modified to include Δn (see Eqs. 11 and 12), then agreement with the exact DDAM solution is improved, but is more divergent for grating slant angle $\phi = 30°$ compared to the first-order approximation of the DDAM solution. Finally, if only one angular deviation from the recording condition is used to represent the extent of Bragg mismatch, as described in Ref. 16, and $\Delta\Omega_{2_{ext}}$ is chosen as the reference angle,[3,16] then the magnitude of volume shrinkage is significantly overestimated for all grating slant angles, whereas if $\Delta\Omega_{1_{ext}}$ is chosen as the reference angle (choice of $\Delta\Omega$ is arbitrary) then a similar overestimation is obtained.

Differential Scanning Photocalorimetry. Differential photocalorimetry (photo-DSC) was utilized to investigate the reaction kinetics of photopolymerization under isothermal conditions of the ULSH-500 holographic recording medium. The fractional extent of cure as a function of pre-imaging fluence and write irradiance was determined to better understand the tradeoff between dynamic range and shrinkage. The fractional extent of photochemical reaction as a function of illumination time, $q(t)/\Delta H_{rxn}$, and fluence was determined for exposure intensities between 0.1 and 10 mW/cm^2 at $\lambda = 514.5$ nm by the method described previously.[1] The intensities used corresponded to those typically employed for both pre-imaging exposure and holographic recording. The fractional extent of reaction increased more rapidly with illumination time as a function of increasing exposure irradiance, shown in the inset of Fig. 6, whereas the total heat evolved was independent (within experimental error) of illumination intensity. The time required to reach 50% reaction, $t_{1/2}$, decreased from 154 seconds for an illumination intensity of 0.11 mW/cm^2 to 7.6 seconds for 10 mW/cm^2. The rate of growth in the extent of reaction is thus seemingly related to the number of initiated chain growths per unit volume, but in a nonlinear manner. The heats of polymerization were between 53 and 59 kJ/mole epoxy, which is in good agreement with literature results for various epoxy resins.[17,18] The fractional extent of evolved heat as a function of exposure fluence, however, shown in Fig. 6, exhibits inverse dependence on irradiance. The fluence required to attain the 50% reaction level, 17.3, 22.6, 36.9, 51.3, and 76.3 mJ/cm^2 for an irradiance of about 0.11, 0.4, 1.0, 4.0, and 10.0 mW/cm^2, respectively, increased with increasing exposure irradiance. If it is assumed that quantum efficiency is independent of irradiance, then these results suggest that diffusion control, such as due to decreased mobility of sensitizer dye molecules in the crosslinked microstructure, increased competition for available monomer, or possibly due to shielding of reactive sites by crosslinked microstructure, may be impeding reaction rates at higher exposure intensity. A reduction in the rate of approach to vitrification as a function of fluence would result, thereby enabling the same final extent of reaction to be attained when illuminating with higher irradiance.

In an effort to quantify the consumption of reactive species occurring during pre-imaging exposure of holographic formulations, calorimetric experiments were performed in which samples were irradiated at a defined intensity for differing periods of time. Accordingly, heat evolution was monitored with time during and after shortened exposures to ascertain the magnitude of dark reaction as a function of fluence. The exposures were carried out at an irradiance of 0.4 mW/cm^2, for times commensurate with that needed to simulate the fluence of pre-imaging exposures used prior to recording holograms of low diffraction efficiency (see below). Results shown in Fig. 7 indicate a significant amount of monomer consumption occurred after cessation of the irradiation. Although the consumption of monomer during the irradiation was relatively linear with exposure, the subsequent dark growth was not linear with time, and the final heats evolved, 85.5, 97.0, and 129.1 J/g for exposures of 9.6, 14.4, and 19.2 mJ/cm^2, respectively, were not a linear function of exposure fluence. The reduction of the extent of reaction with increased exposure fluence is likely the result of increased viscosity of the photopolymer recording medium, such that termination processes can become competitive with chain growth and/or crosslinking chemistry. The fractional extent of heat evolved at the termination of

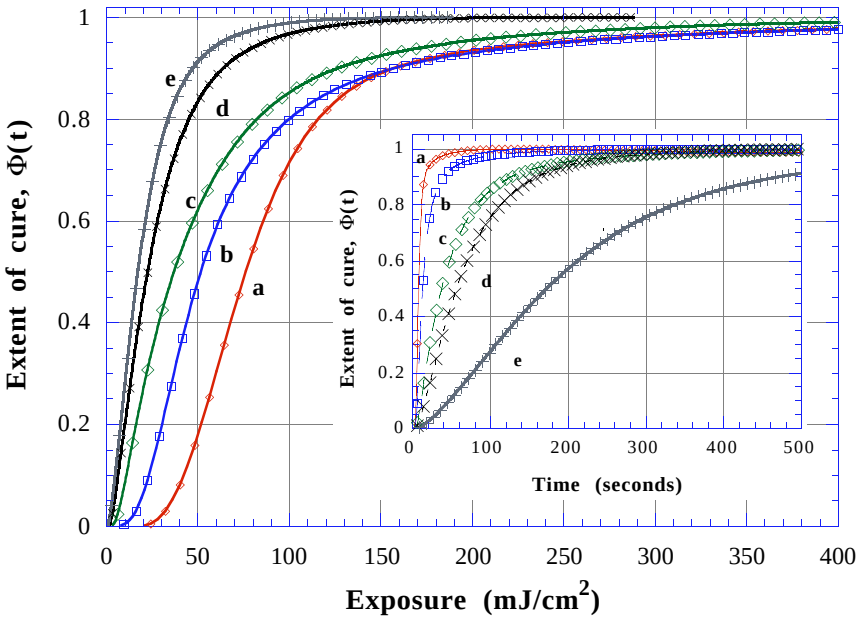

Figure 6. Fractional extent of energy evolved, $\Phi(t)$, during photochemically initiated polymerization of CROP holographic recording medium, ULSH-500, as a function of fluence in mJ/cm^2 and time in seconds (inset figure) for varying levels of incident irradiance from argon laser radiation at 514.5 nm: (a) 10.0 mW/cm^2; (b) 4.0 mW/cm^2; (c) 1.0 mW/cm^2; (d) 0.4 mW/cm^2; and (e) 0.1 mW/cm^2. Data were collected at intervals of 0.4 s, and a subset of total data points is plotted.

exposure, relative to the final value attained during dark growth over a time period of 10 minutes, was 0.41, 0.59, and 0.61 for an exposure fluence of about 9.6, 14.4, and 19.2 mJ/cm^2, respectively. Accordingly, the amount of shrinkage in low diffraction efficiency holograms, and thus the angular deviation, depends not only on the intensity used for pre-imaging exposure and the exposure fluence, but also on the extent of dark growth prior to imaging. Similarly, the dynamic range will be impacted by both the extent of pre-imaging exposure and the subsequent dark growth. Therefore, a wait time of 10 minutes, between the pre-imaging exposure and holographic recording, was utilized as a protocol for experiments in which holograms of low diffraction efficiency were recorded. This ensured that a consistent steady-state dark growth was attained prior to holographic recording, thereby eliminating additional variability from the determination of shrinkage in holograms of low diffraction efficiency.

Shrinkage in Slant Fringe Holograms Recorded with Low Diffraction Efficiency. Additionally, and of greater interest for applications such as holographic optical data storage, are results obtained for holograms recorded in CROP photopolymer to low diffraction efficiency (i.e., on the order of 0.1% to 1%). Previous studies have addressed the dependence of dynamic range on hologram thickness and the need for exposure scheduling when multiplexing equal strength holograms in photopolymer films.[19] These studies were carried out using a non-slant recording geometry due to the significant shrinkage exhibited by photopolymers based on conventional free radical polymerization. As mentioned above, shrinkage causes angular deviations in the Bragg profile of slant fringe holograms that can exceed the angular bandwidth of holograms with thickness greater than 100 μm, even for moderate slant angles. Moreover, the magnitude of $\Delta\Omega_{1_{ext}}$ and $\Delta\Omega_{2_{ext}}$ is dependent on the slant angle, as shown in Fig. 4. Image reconstruction (readout) of a single image, which comprises multiple gratings, (e.g., Fourier images) is therefore likely to result in lack of image fidelity and/or distortion unless the shrinkage is reduced to extremely low levels. Accordingly, holograms recorded to low diffraction efficiency in the photopolymer holographic recording material ULSH-500 were flood exposed subsequent to imaging and prior to measurement to simulate the densification effect that occurs when holograms are multiplexed until the entire dynamic range of the medium is consumed. The angular deviations measured according to this experimental protocol are expected to represent the maximum values exhibited when recording is carried out with angle multiplexing schemes (i.e., the first few holograms recorded will display larger shifts than later recorded holograms due to densification effected by later recording events).

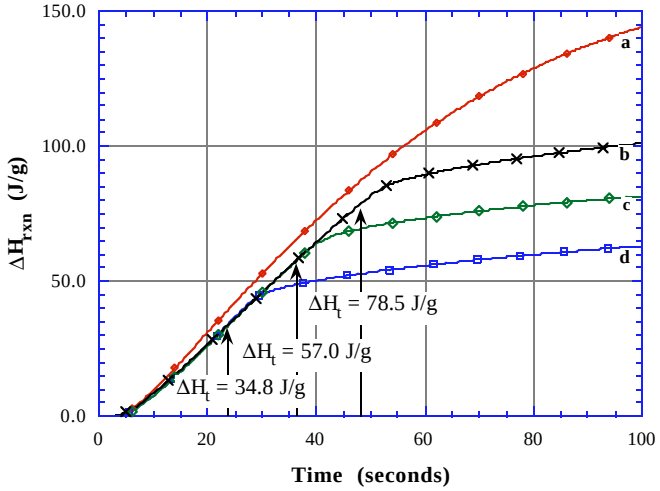

Figure 7. Energy evolved during photochemically initiated polymerization of CROP holographic recording medium (ULSH-500) at termination of exposure from argon laser radiation at 0.4 mW/cm^2 for exposure fluence of: (a) control (240 mJ/cm^2); (b) 19.2 mJ/cm^2; (c) 14.4 mJ/cm^2; and (d) 9.6 mJ/cm^2. Fractional extent of heat evolved at termination of exposure (shown by arrows) relative to final value attained resulting from subsequent dark growth is (a) 1.0; (b) 0.61; (c) 0.59; and (d) 0.41.

Good angular selectivity with sinc function behavior was obtained in holograms of low diffraction efficiency by use

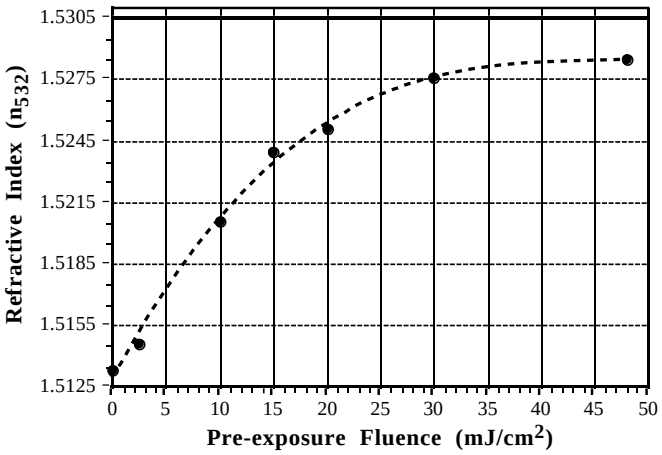

Figure 8. Index of refraction, n_{532}, as a function of non-holographic pre-imaging exposure fluence in mJ/cm^2. Values of n_d and the dispersion, K, were measured under dark room conditions and then utilized to calculate values of n at the read wavelength, 532 nm. The maximum value of n_{532} at complete reaction is solid line at n =1.5305.

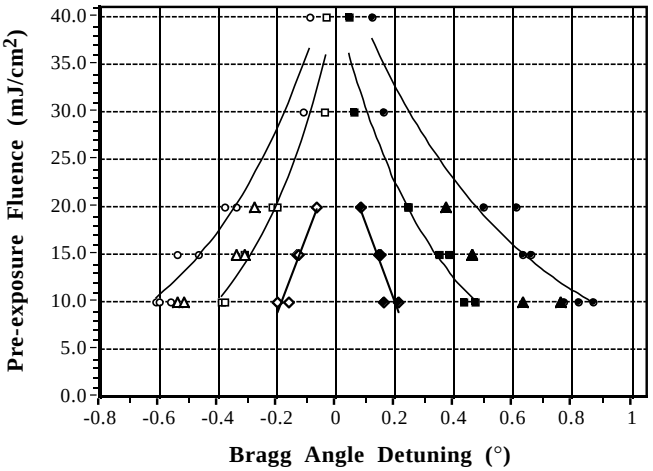

Figure 9. Plot showing angular deviations from Bragg matching condition, $\Delta\Omega_{1_{ext}}$ (open symbols) and $\Delta\Omega_{2_{ext}}$ (filled symbols), as a function of internal slant angle, ϕ, and pre-imaging exposure fluence, for slant fringe plane-wave volume holograms recorded to low diffraction efficiency, and subsequently flood exposed with a fluence of about 100 mJ/cm^2 at λ = 532 nm to consume the full dynamic range of the CROP photopolymer, ULSH-500. Recording slant angle ϕ was about 5°(◊), (♦); 10°(□), (■); 15° (Δ), (▲); and 20°(○), (●), respectively. Solid lines represent curve fits.

of a low-fluence pre-imaging exposure prior to recording. Experimental results and calculated values are listed in Table III for slant angle $\phi \cong 10°$ and 20° for various pre-imaging exposure conditions. A plot of the increase in refractive index as a function of increasing pre-imaging exposure fluence is shown in Fig. 8. The values of n_{532}, which were calculated from the measured values, n_d, and dispersion, K, were used for the initial refractive index at the onset of recording for calculations of dimensional change in the xz plane. The final value of the refractive index, attained after a flood post-exposure, is shown by the solid line at n = 1.5305. Angular deviations for grating slant angles of $5° \leq \phi \leq 20°$ are shown in Fig. 9 for a range of pre-imaging exposure conditions. Two data points are plotted for certain slant angle and pre-exposure conditions to indicate the range of values obtained for angular deviations across multiple experiments. Figure 10 shows angular selectivity profiles of $\Omega_{1_{ext}}$ and $\Omega_{2_{ext}}$ for an internal slant angle $\phi \cong 20°$, where the pre-imaging exposure fluence was 20 mJ/cm^2 at λ = 514.5 nm and holographic recording provided a diffraction efficiency of about 0.2%. Deviations from the Bragg matching condition were –0.28° and +0.39° (sign defined above) for $\Delta\Omega_{1_{ext}}$ and $\Delta\Omega_{2_{ext}}$, respectively, and sinc-function-like behavior was exhibited. The hologram in Fig. 10 was recorded in a medium comprising an increased ratio of binder to reactive components, and thus the angular deviations were reduced further from those plotted in Fig. 9. Holograms recorded to near saturation exhibit smaller angular deviations than their low diffraction efficiency counterparts. A comparison example is listed for $\phi \cong 20°$, where the entry in Table I is for a hologram recorded to 90% diffraction efficiency, while that in Table III, for the case of no pre-imaging exposure, is for a hologram which was recorded to only 0.02% diffraction efficiency and then subsequently exposed to a flood exposure at the write wavelength to complete polymerization.

A significant reduction in the angle shifts accompanying hologram formation was realized by carrying out pre-imaging exposures. A pre-imaging exposure fluence between 30 and 40 mJ/cm^2 was sufficient to reduce the magnitudes of the angular deviations to ≤ 0.1°, even for a grating slant angle of $\phi \cong 20°$. Components of the grating vector, **K**, in the x and z directions, as a function of pre-imaging exposure fluence, were calculated from the increase in refractive index and the angular deviations shown in Figs. 8 and 9, respectively. The corresponding values for the relative change in the transverse (perpendicular to film plane) component of the grating vector, $-\Delta K_z/K_{z,i}$, for $\phi \cong 20°$ decreased to ≤0.2% for a pre-imaging exposure fluence ≥30 mJ/cm^2. For $\phi \cong 10°$ the values of $-\Delta K_z/K_{z,i}$ decreased by factors of 7.5 and 11.2 for pre-exposure fluence of 30 and 40 mJ/cm^2, respectively, relative to that displayed at a pre-imaging exposure of 20 mJ/cm^2. The magnitude of the shrinkage in the transverse direction can thus be diminished to acceptably low levels for angle multiplexing holograms of low diffraction efficiency. The calculated material volume shrinkage for $\phi \cong 10°$ was 0.11%, 0.23%, 1.11%, and 1.97% for pre-imaging exposure fluences of 40, 30, 20, and 10 mJ/cm^2, respectively, while for $\phi \cong 20°$ it was 0.09%, 0.21%, 0.94%, and 0.94% for 40, 30, 20, and 10 mJ/cm^2, respectively. The effect of an extensive post-imaging flood exposure (i.e., 6000 mJ/cm^2 at the write wavelength) on the magnitude of $\Delta\Omega_{1_{ext}}$ and $\Delta\Omega_{2_{ext}}$, as compared to the fluence required to consume the dynamic range associated with observation of holographic activity, that being 150 to 200 mJ/cm^2, was minimal. The extensive flood exposure caused an additional angular shift of 0.04° and 0.11° for $\Delta\Omega_{1_{ext}}$ and $\Delta\Omega_{2_{ext}}$, respectively, for a hologram recorded with grating slant angle $\phi \cong 20°$ after using a pre-imaging exposure of 20 mJ/cm^2. Moreover, angular selectivity profiles of holograms with low diffraction efficiency exhibited the expected sinc function behavior with minimal background uplift for pre-exposure fluence of ≥10 mJ/cm^2 and good image uniformity was observed.

Figure 11 shows representative angular selectivity profiles of $\Omega_{1_{ext}}$ and $\Omega_{2_{ext}}$ for an internal slant angle $\phi \cong 10°$, where the pre-imaging exposure fluence was 15 mJ/cm^2 at λ = 514.5 nm and holographic recording provided a diffraction efficiency of about 1.2%. The angular deviations, which were 0.16° and 0.16°, respectively, from the Bragg matching condition, were diminished from that listed in Table III for a 20 mJ/cm^2 pre-imaging exposure. A reduc-

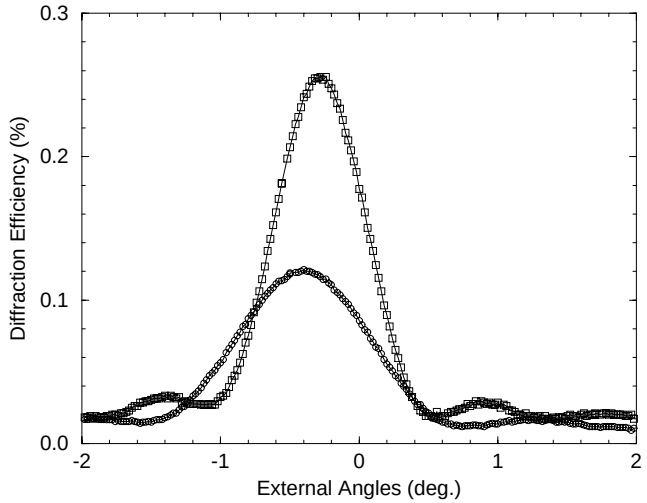

Figure 10. Angle selectivity profiles of $\Omega_{1_{ext}}$ (□) and $\Omega_{2_{ext}}$ (○) showing angular deviations, $\Delta\Omega_{1_{ext}}$ and $\Delta\Omega_{2_{ext}}$, from Bragg matching condition for slant fringe hologram with internal slant angle, ϕ, of ≅ 20° recorded in a formulation with increased binder content. Pre-imaging exposure fluence was 20 mJ/cm² at λ = 514.5 nm. Resolution of data collection was 0.001° and increment was 0.02°.

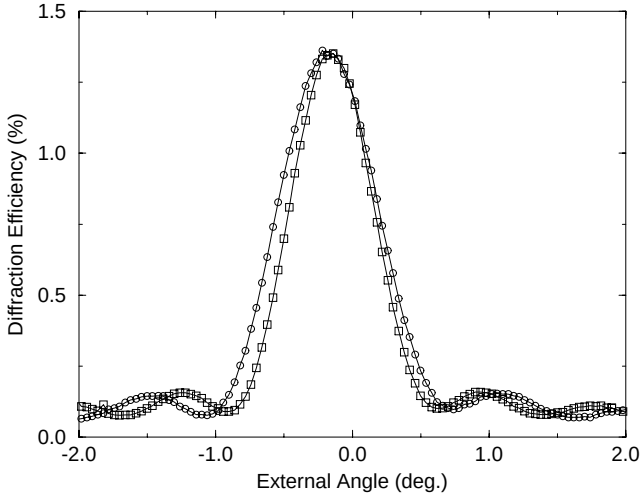

Figure 11. Angle selectivity profiles of $\Omega_{1_{ext}}$ (□) and $\Omega_{2_{ext}}$ (○) showing angular deviations, $\Delta\Omega_{1_{ext}}$ and $\Delta\Omega_{2_{ext}}$, from Bragg matching condition for slant fringe hologram which was recorded with internal slant angle, ϕ, of ≅ 10°, after first holographically imaging at ϕ ≅ 20°. Pre-imaging exposure fluence (see text) was 15 mJ/cm² at λ = 514.5 nm. Resolution of data collection was 0.001° and the increment plotted is 0.02°.

TABLE III. Measured Angular Deviations from the Bragg Matching Condition and Calculated Values of the Relative Change in the Grating Vector Component Along the Transverse (Thickness) Direction for Plane-Wave Slant Fringe Holograms Recorded, After a Pre-Imaging Exposure, with Low Diffraction Efficiency.

ϕ_0^* (°)	Pre-fluence† (mJ/cm²)	$\Delta K_z / K_{z,i}$‡	$\Delta\Omega_{2_{ext}}$¶ (°)	$\Delta\Omega_{1_{ext}}$¶ (°)	η§ (%)
$\Omega_{1_{ext}}$ = -16°, $\Omega_{2_{ext}}$ = 48°					
19.89	0	0.0221	+ 1.30	- 0.83	~ 0.02
19.85	10	0.0122	+ 0.79	- 0.59	~ 0.8
19.79	20	0.0123	+ 0.66	- 0.50	~ 1.3
19.75	30	0.0020	+ 0.16	- 0.11	~ 0.12
19.74	40	0.0014	+ 0.12	- 0.09	~ 0.03
$\Omega_{1_{ext}}$ = -0.4°, $\Omega_{2_{ext}}$ = 31.6°					
9.95	10	0.0198	+ 0.45	- 0.39	~ 0.5
9.92	20	0.0112	+ 0.25	- 0.22	~ 1.0
9.90	30	0.0015	+ 0.06	- 0.04	~ 0.12
9.89	40	0.0010	+ 0.042	- 0.034	~ 0.01

* ϕ_0 is internal slant angle at onset of recording where $n_{0,532}$ is a function of pre-imaging exposure fluence (see Fig. 6). Recording geometry was kept constant for each set of slant fringe holograms, and thus slight variation in ϕ arises from the change in refractive index of the recording medium. The recording and readout wavelengths were λ = 532 nm.

† Pre-imaging exposures were carried out with radiation from an Ar^+ laser at λ = 514.5 nm.

‡ $\Delta K_z/K_{z,i}$ is the relative change in the grating vector along the transverse (thickness) direction, which is the negative of the material shrinkage, $-\Delta\Lambda_z/\Lambda_z$, in the *z* direction, independent of slant angle.

¶ $\Delta\Omega_{1_{ext}}$ and $\Delta\Omega_{2_{ext}}$ are deviations of the external signal and reference beam read angles from the Bragg matching condition (see Fig. 3 and equations in text).

§ η is the diffraction efficiency measured during readout of angular selectivity at λ = 532 nm.

tion in the magnitude of the angular deviations occurred because a hologram with slant angle ϕ ≅ 20° was first recorded using an exposure fluence of about 3 mJ/cm² at λ = 532 nm and this was followed by a subsequent holographic recording in the same area for a slant angle ϕ ≅ 10°. This result demonstrates the effect of variable levels of shrinkage, even for a low shrinkage recording medium, which may be expected during angle multiplexing when later recording events are imaged in an increasingly denser recording medium.

Angle Multiplexing of Slant Fringe Holograms. Multiplexing schemes, such as angle multiplexing of slant fringe holograms, provide a means of increasing storage capacity. Angle multiplexing was carried out in ULSH-500 by rotating the sample by 2.5° increments and recording low diffraction efficiency holograms at each angle with a fixed external interbeam angle of 32°. In Fig. 12 results are shown for angle multiplexing N = 30 slant fringe holograms. A pre-imaging exposure was not used; the first hologram was recorded with an exposure fluence of about 15 mJ/cm² resulting in a relatively high diffraction efficiency of 13%. Subsequent holograms were recorded starting with a rotation of 15° (corresponds to ϕ ≅ 20°) from the first recording angle, thereby ensuring minimal crosstalk from the side lobes of the first hologram. A coarse manual scheduling was imposed in an effort to record holograms with similar diffraction efficiency. Accordingly, the exposure fluence was 1.5 mJ/cm² for hologram #2, 0.9 mJ/cm² for holograms #3 through #19, and then increased in monotonic fashion for the subsequent recording of holograms #20 through #30. A flood post-exposure was carried out using an additional fluence of about 50 mJ/cm² at the write wavelength of 532 nm. In Fig. 12 an angular profile scan, obtained with a resolution of 0.4°, is shown of all 30 angle multiplexed holograms. Holograms #6 and # 7, which were angularly separated by only about 1°, instead of 2.5°, were still resolved. The envelope of the manifold of diffraction efficiency with hologram number, N, decreased from an external angle of about 2° to 46° due to the lack of more accurate scheduling. The inset figure shows a magnified view of the angular profiles for each hologram that exhibited a diffraction efficiency less than 0.4%. The diffraction efficiency envelope exhibits minimal background uplift and minimal crosstalk, except for holograms #6 and #7, which had the smaller angle separation, and holograms #29 and #30, due to the significantly higher diffraction efficiency

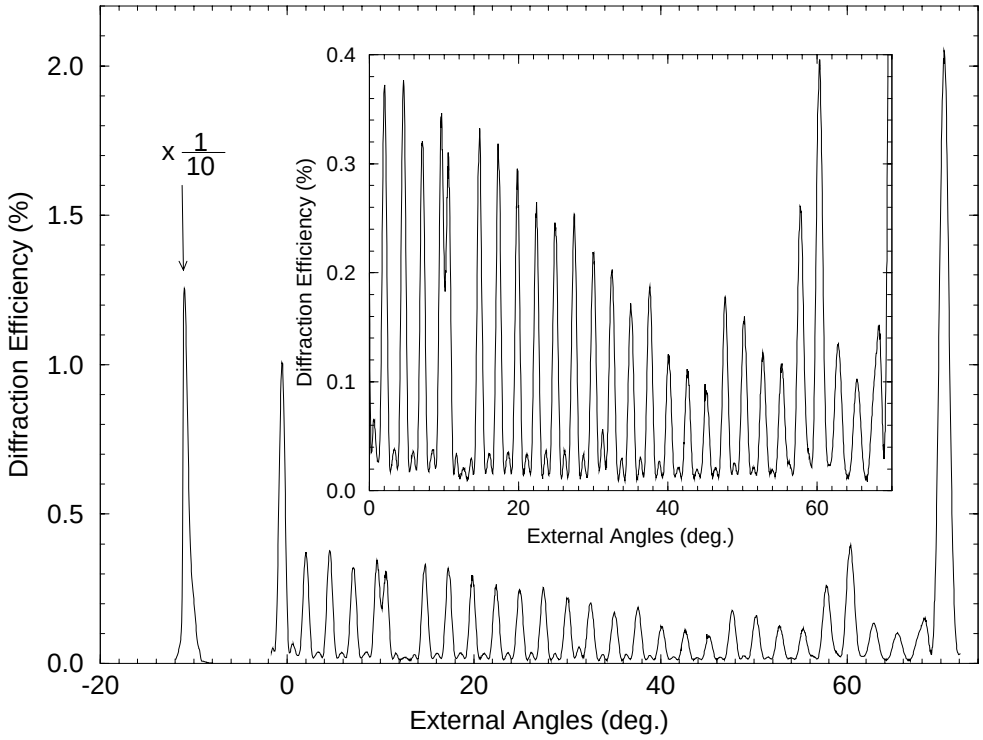

Figure 12. Example of angular multiplexing in a 130-μm-thick sample of ULSH-500. The sample was not pre-exposed. Multiple plane-wave holograms were recorded by rotating the sample plate by increments of 2.5° through a range of angles comprising internal slant angles, ϕ, between about -25° and +25°. The external interbeam angle was 32°, and the write irradiance was about 3.0 mW/cm^2 at the condition of bisecting recording angles where the beam ratio was 1:1. A coarse recording schedule was implemented (see text).

of hologram #30. The last hologram recorded (#30) was imaged with greater fluence to demonstrate that incomplete consumption of the dynamic range existed, and thus it exhibited a diffraction efficiency which was about 20 times greater than that of the previous hologram. The angular deviation, $\Delta\Omega_{1_{ext}}$, of hologram #2 was 0.54° for a slant angle ϕ of 20°, whereas for hologram #28, which had the same slant angle, the value of $\Delta\Omega_{1_{ext}}$ was 0.35°. The decrease noted in the magnitude of the angular deviation is attributed to densification of the recording medium that occurs during angle multiplexing.

Analysis of Background Uplift from Nonuniform Gratings. To achieve lower recording threshold and increased sensitivity required an approach that involved increasing both photoacid and sensitizer concentration, where the latter resulted in increased absorption. Although this indeed lowers the recording threshold and increases recording sensitivity (while still achieving close to 100% diffraction efficiency), the angular selectivity curves of the recorded holograms sometimes deviated considerably from the ideal sinc^2 function line shape predicted by coupled wave equations.[20] In particular, the nulls (or rather, the minima) of the selectivity curve no longer diminished to zero diffraction efficiency. In this article, however, the terminology "null" will be used with the understanding that it is no longer equated with zero diffraction efficiency. This is of interest because Bragg selectivity is an important property in many applications of holography, such as data storage utilizing angle or wavelength multiplexing recording schemes.

The departure from an ideal sinc^2 function is caused at least partially by the non-uniformity of the gratings recorded in the material. As a result of the large absorption coefficient arising from the sensitizer, the amount of transmitted light available for absorption by the sensitizer molecules during recording diminishes with depth as light penetrates into the film of the recording medium. Accordingly, the grating strength recorded (and more generally, the absorption coefficient) throughout the depth of the media will not be uniform, and this effect needs to be taken into account in the coupled wave analysis. Related cases have been studied in several articles.[13,21–29] Herein, the results relevant to the photopolymer holographic recording material, ULSH-500, are summarized and the resultant implications for holographic data storage systems that use angle or wavelength multiplexing schemes are considered. Although this article concentrates mostly on angle multiplexed transmission holograms, the results can be easily generalized.

The formalism discussed here starts with Kogelnik's coupled wave equations,[20] (The notation used here is different from Kogelnik's). Let z be the direction normal to the photopolymer film and x be the direction perpendicular to z. Let E_1 and E_2 represent the amplitude of the reference beam and diffracted beam, respectively. Both are assumed to be functions of z. Let $\Omega_{i_{\text{int}}}$ be the angle between the direction of propagation of E_i and the z axis (see Fig. 1). The recorded grating is assumed to be of the form

$$n(x,z) = n_0 + n_1(z)e^{-j(K_x x + K_z z)} + c.c., \tag{13}$$

where c.c. represents the complex conjugate, $\mathbf{K} = (K_x, 0, K_z)$ is the grating vector and the average index of refraction of the media is n_0. In general n_1 is a function of z. The recording media exists in the region between $z = 0$ and $z = L$. For transmission holograms, a reference beam E_2 is

applied at $z = 0$ and E_1 is determined at $z = L$. The diffraction efficiency of the grating is then $\eta = |E_1(L)/E_2(0)|^2$, assuming that there is no absorption during reconstruction of the hologram. A non absorption state can be achieved either by bleaching of the dye prior to readout or because the material does not absorb at the wavelength of the light used for readout.

Following Kogelnik's coupled wave analysis, E_1 and E_2 satisfy the following equations:

$$\cos\Omega_{1_{int}} \frac{dE_1}{dz} = jk\left(\frac{n_1 k}{n_0 k_1}\right)E_2 + j\left(\frac{k^2 - k_1^2}{2k_1}\right)E_1, \qquad (14)$$

$$\cos\Omega_{2_{int}} \frac{dE_2}{dz} = jk\left(\frac{n_1}{n_0}\right)E_1, \qquad (15)$$

where $k = 2\pi n_0/\lambda$ and $\Omega_{2_{int}}$ is the angle between the reference beam and the z axis (all angles here refer to internal angles inside the media unless otherwise noted). The direction of the reference beam is $\mathbf{k}_2 = (k\sin\Omega_{2_{int}}, 0, -k\cos\Omega_{2_{int}})$ and the direction of the diffracted beam is $\mathbf{k}_1 = \mathbf{k}_2 + \mathbf{K}$. Note that while $k_2 = |\mathbf{k}_2| = k$, in general $k_1 = |\mathbf{k}_1|$ is not equal to k. Let

$$\xi = \frac{k^2 - k_1^2}{2k_1\cos\Omega_{1_{int}}} \qquad (16)$$

For angle multiplexing, ξ is proportional to the change in angle and for wavelength multiplexing, it is proportional to the change in wavelength.

First consider the case where the diffraction efficiency is low. This is of particular interest to holographic data storage, because it is usually desirable to multiplex colocationally as many holograms as possible to maximize storage capacity. This implies that the diffraction efficiency of each individual hologram is necessarily low, so that the reference beam E_2 changes very little throughout the thickness of the material. Accordingly, E_2 is approximately constant and thus this condition will be referred to as the undepleted reference beam approximation. Consequently, the Bragg selectivity curve (angle or wavelength) is the square of the absolute value of the Fourier transform of the function $n_1(z)$ (between $z = 0$ and $z = L$; the change is zero outside this region), with the appropriate changes in scale. It is under this approximation, and assuming that n_1 is a constant (i.e., constant grating strength), that the familiar sinc^2 function characteristic is obtained, since the Fourier transform of a rectangle gives a sinc function. If $n_1(z)$ is not a constant, then its Fourier transform is no longer a sinc function, and thus the uplift of nulls, etc., will be observed in the actual Bragg selectivity curves.

For larger diffraction efficiencies, the approximation of E_2 as a constant is no longer appropriate. In general, it is not possible to find a solution for an unspecified $n_1(z)$ except numerically. The diffraction efficiency may be expressed in terms of an integral of $n_1(z)$ at the Bragg peak,[25] but for off-Bragg peak conditions there is no known corresponding expression. Note, however, that even for larger diffraction efficiencies, off the Bragg peak where the diffraction efficiency is low, the undepleted reference beam approximation still holds.

It may be expected that additional information can be ascertained by flipping the hologram backward (after the grating is recorded) and measuring the resultant Bragg selectivity profile. This is not the case, however, even though the grating strength profile would be inverted and the strength would thus increase rather than decrease. Although the analytical solution to the coupled wave equations for a generalized $n_1(z)$ cannot be found, it can be shown that the Bragg selectivity curve is identical if the hologram is flipped backward [mathematically changing $n_1(z)$ to $n_1(L - z)$], and this is indeed what was observed with the photopolymer holographic recording medium, ULSH-500.

As a simple model for a non-uniform grating, one can assume an exponentially decaying $n_1(z)$:

$$\frac{n_1(z)}{n_0} = \frac{n_{10}}{n_0}e^{-\alpha z}, \qquad (17)$$

where n_{10} is the value of n_1 at the front plane ($z = 0$) of the hologram, and α is a constant which represents the extent of the exponentially decreasing index modulation through the thickness z. Although the solution to the coupled wave equation for $n_1(z)$ can be expressed in terms of Bessel functions,[21] the expression is complicated. In Fig. 13 diffraction efficiency, η, versus u, where $u = \xi L/2$, is shown for two examples of the calculated Bragg selectivity curve, using both the undepleted reference beam approximation as well as the exact solution by numerical integration. For the case where $kn_{10}/n_0 = 2$, the undepleted reference beam approximation causes the diffraction efficiency to be larger than 1 near Bragg incidence ($u = 0$), which confirms that the approximation is only appropriate for small diffraction efficiencies. In the region of the first side lobe, however, the approximation is already fairly good, even though the position of the first null (or minimum) is slightly different from the value of u obtained by numerical integration. When $kn_{10}/n_0 = 1$, the result obtained with the undepleted reference beam approximation is in better agreement with that from numerical integration, as expected.

It is apparent from Fig. 13, that the nulls of the angular selectivity curve, obtained using the coupled wave analysis, are no longer at zero diffraction efficiency. Additionally, as the half value of the decline in grating strength, defined as $a = \alpha L/2$, increases the magnitude of the nulls increase and their position moves further from the Bragg peak position at $u = 0$. Figure 14 shows, from numerical calculations of η/η_{max} versus u, that the nulls disappear for sufficiently large $aL/2$ and are no longer resolved from the Bragg peak. For weak gratings, where the undepleted reference beam approximation can be applied, the values of a at which the m^{th} null disappears, defined as a_m, is approximately independent of n_{10}. Moreover, the m^{th} null disappears for $a \geq a_m$, and the selectivity curve becomes monotonically decreasing for that region of ξ. The values of a_m for the first few nulls, $m = 1$ to $m = 5$, are $a_m = 1.0572$, 1.3333, 1.5074, 1.6455, and 1.749 for $m = 1$, 2, 3, 4, and 5, respectively.

m	a_m
1	1.057
2	1.333
3	1.507
4	1.645
5	1.749

As mentioned previously, n_1 varies with depth for the photopolymer holographic recording medium. If it is assumed that the decay of n_1 is exponential (Eq. 17), then the

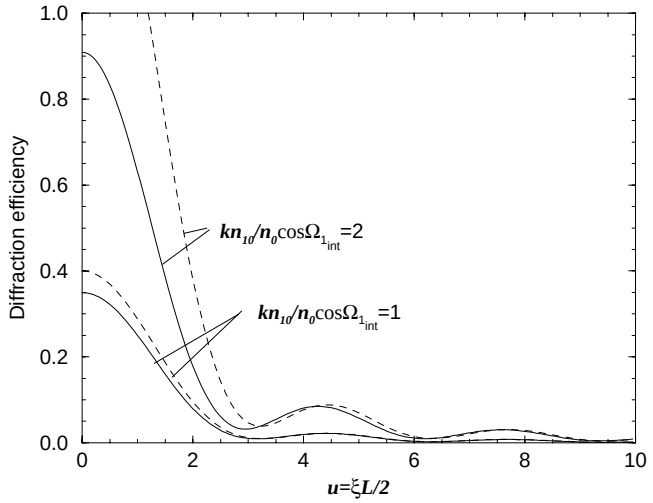

Figure 13. Selectivity curve of diffraction efficiency versus u for $a = \alpha L/2 = 0.5$ from numerical integration (—) and the undepleted reference beam approximation (- - -), where $\Omega_{1_{int}} = \Omega_{2_{int}}$.

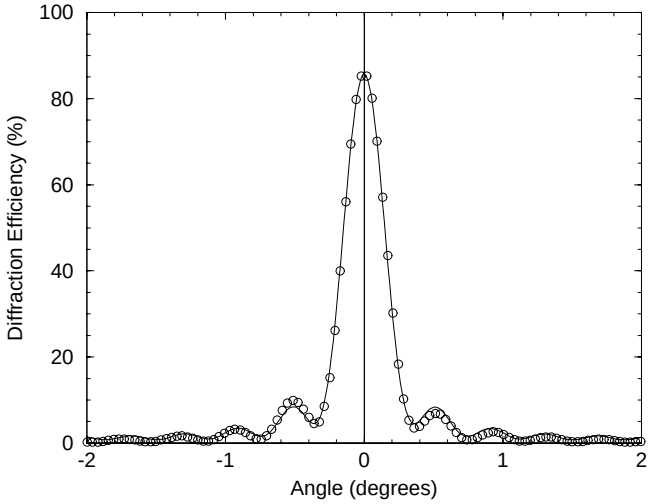

Figure 15. Comparison between theoretical result (—), from coupled wave analysis, and angle selectivity curve from experimental data (○), where $\Omega_{1_{ext}} = \Omega_{2_{ext}} = 31°$(external angle), $n_0 = 1.5$, and $\lambda = 633$ nm. Data fit to theory by using $a = \alpha L/2 = 0.62$, $L = 154$ μm, and $n_{10} = 0.0013$.

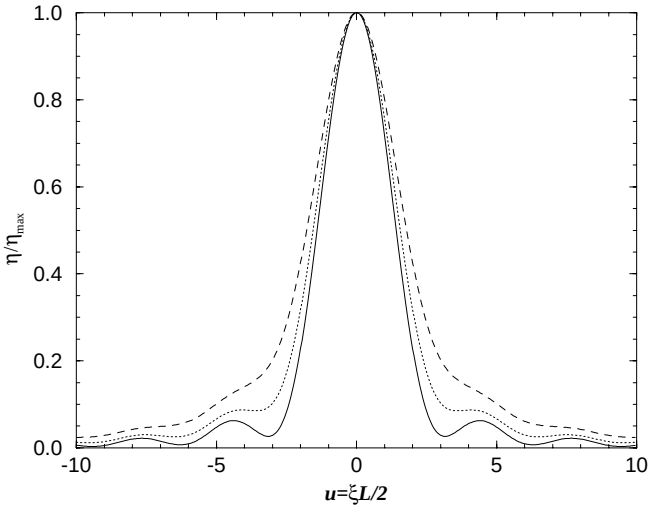

Figure 14. Normalized diffraction efficiency, η/η_{max}, versus u for $a = \alpha L/2 = 0.5$ (—), 1.0 (····), and 1.5 (- - -). [$\Omega_{1_{int}} = \Omega_{2_{int}}$ and $kn_{10}/(n_0 \cos \Omega_{1_{int}}) = 2$].

theoretical results can be fit to the experimental data when the amount of decay, αL, is small. An example case is shown in Fig. 15, where the reconstruction angles were $\Omega_{1_{ext}} = \Omega_{2_{ext}} = 31°$ (external angle), $n_0 = 1.5$, and $\lambda = 633$ nm. The data can be fit to theory by taking $a = \alpha L/2 = 0.62$, $L = 154$ μm, and $n_{10} = 0.0013$, whereas the value of material thickness obtained from direct measurement (using a profilometer) was $L = 136$ μm. This discrepancy could be because direct measurement of L was performed at the edge of the hologram sample, whereas the angle selectivity curve was measured at the center of the sample, suggesting that variations might exist in the coating thickness across the sample. It is more likely, however, that the assumption of n_1 exhibiting a exponential decline with depth is only approximate. For instance, there were cases where the angle selectivity curve, such in Fig. 16, could not be adequately fit with the assumption that n_1 decays exponentially throughout the thickness. In such cases, the rise of the side lobes are too pronounced to be explained by the exponentially decaying n_1 model, which suggests that the variation in n_1 can be more complicated than defined by the model of Eq. 17 and is likely effected by the nonlinear response of the material.

To further test the hypothesis that the uplift of the nulls is caused by a non-uniform grating profile, gratings were recorded in samples of various thicknesses using the same photopolymer formulation. The samples thus had the same sensitizer dye concentration and absorption coefficient, but the thinner samples exhibit reduced absorbance, and thus a more uniform grating profile was expected. In this manner the number of initiated reactions per unit volume is maintained for a given intensity. In thinner samples, however, a diminished amount of light would be absorbed before it reached the back plane of the sample, and thus the amount of light absorbed throughout the sample thickness would be more uniform during holographic recording. This was confirmed experimentally, and examples of results for measured angular selectivity profiles of two different coating thicknesses are shown in Figs. 17(a) and (b), together with the conventional prediction from Kogelnik's[20] coupled wave analysis. It is apparent that the measured profiles increasingly exhibit sinc^2 function behavior as the coating thickness of the hologram is further reduced. Note that the background uplift in the region of the first nulls is barely discernible for the thinnest hologram recorded and is more readily apparent in the profile of the slightly thicker hologram.

Holographic storage systems require large numbers of holograms to be stored co-locationally to maximize storage capacity. It is known that for optically erasable materials (e.g., photorefractive crystals), which exhibit diffraction efficiencies that erase exponentially with exposure, and for materials which exhibit a recording regime where index modulation increases linearly with fluence, the efficiency of each hologram scales as $1/M^2$, where M is the number of holograms recorded co-locationally.[30] Generally, M is large, hence the diffraction efficiency of individual holograms is small, and it is therefore reasonable to assume that the undepleted reference beam approximation is applicable.

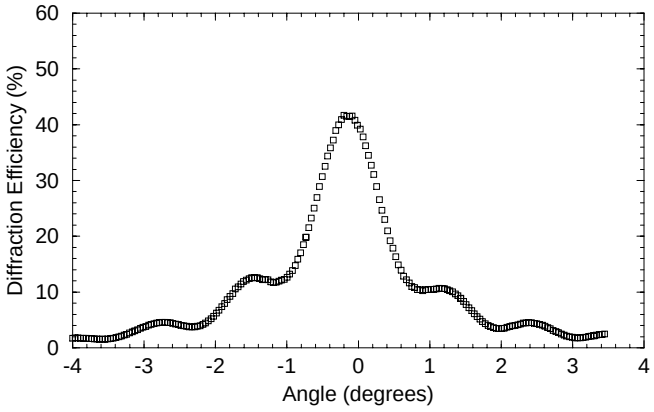

Figure 16. Example of experimental result for angle selectivity curve where the angle profile of diffraction efficiency does not fit the exponentially decaying index modulation (n_1) model.

For either angle or wavelength multiplexing, the diffraction efficiency η is proportional to the square of the Fourier transform of $n_1(z)$, with argument ξ from Eq. 16 either proportional to ΔΩ or Δλ. In either case, to record multiplexed holograms, it is customary to write adjacent holograms at the 1st null of the selectivity curve in order to minimize crosstalk and maximize storage capacity. Assuming that the decay of n_1 is exponential (Eq. 17), it is important to know what amount of the crosstalk noise arises from the uplift in the nulls in the selectivity curve, so that the signal-to-noise ratio (SNR) can be optimized.

Assuming that $\alpha L/2$ is small, the angular selectivity curves deviate minimally from a sinc^2 function. For nonzero α the nulls of the angle selectivity curve will no longer be at zero diffraction efficiency. It can be shown[31] that for small values of a the m^{th} minimum (or null) of the angle selectivity curve is offset from $m\pi$, which are the zeroes of the sinc^2 function, by an amount, v_m, expressed as

$$v_m = \frac{\alpha^2 L^2}{4m\pi} \tag{18}$$

and the value at the m^{th} null (normalized by the maximum peak value of the selectivity curve, $|F_0|$) is

$$\left|\frac{F_m}{F_0}\right|^2 = \left(\frac{a}{m\pi}\right)^2, \tag{19}$$

where the above expressions are truncated at second order approximations of a. Thus, both the offset of the null positions and the diffraction efficiency at the null values increase quadratically with $a = \alpha L/2$.

The approximations stated above for the value of diffraction efficiency at the nulls, as well as the magnitude of the offset, are plotted in Figs. 18 and 19, respectively, for m = 1, 2, and 3, together with results from the numerical solution of the modified coupled wave analysis. The estimate for the diffraction efficiency at the nulls, shown in Fig. 18, holds fairly well up to a = 0.4 for the worst case of m = 1, and for $m \geq 3$ the approximation is commensurate with the numerical solution for $a \leq 1$. The estimate for the offset from $m\pi$, shown in Fig. 19, also holds fairly well up to a = 0.4 for the worst case of m = 1, whereas for higher m , although the deviation from the numerical solution is still better than for m = 1 at $a \geq 0.4$, it is not quite as good as above. The deviation in the latter, however, is relative to $m\pi$, and thus the error in the offset at the null only represents a small fraction of the grating strength at the actual null. Since the diffraction efficiency changes minimally in the region near the null, the effect upon the estimate of the angular selectivity curve is small provided that a is less than about 0.7, even for the case of m = 1.

The implications of using angle or wavelength multiplexing for holographic data storage are important. If adjacent holograms are recorded at the first nulls of their immediate neighbors, then the cross-talk contributions to the diffraction intensity profile are F_1, F_2, ..., etc. This is not precisely true, because the nulls of multiplexed holograms do not exactly coincide with one another,[32,33] and thus the results here only serve as an approximation. To obtain the total crosstalk contribution to one particular hologram from all other multiplexed holograms requires a summation of the F_m terms, for m = ..., -2, -1, 1, 2, ..., to obtain the amplitude and then the square is taken to obtain intensity:

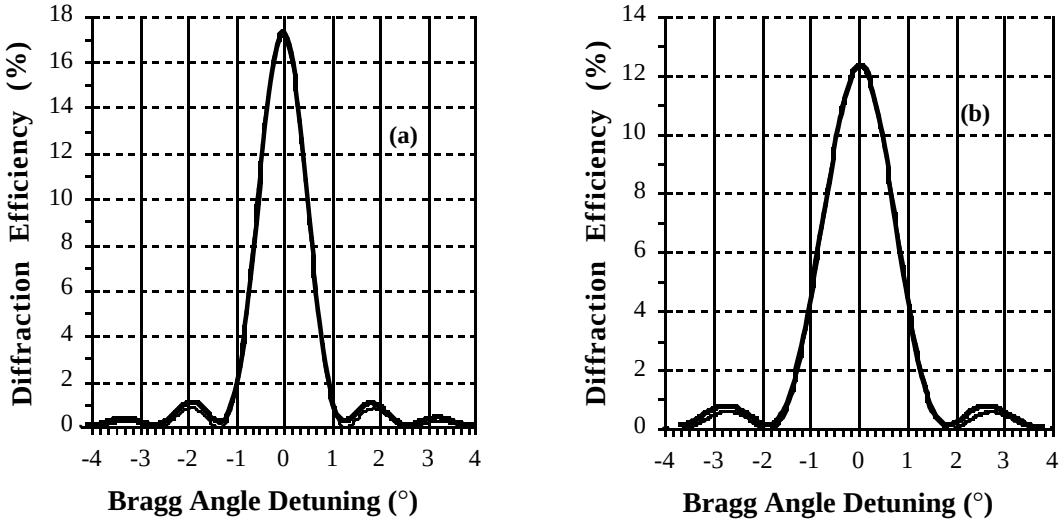

Figure 17. Angle selectivity profiles of thinner non slant plane-wave holograms (▬). Experimental data according to the classical Kogelnik analysisis, (—), corresponds to holograms with a thickness of 45 μm and $n_1 = 1.80 \times 10^{-3}$ for (a), and a thickness of 31 μm and $n_1 = 2.219 \times 10^{-3}$ for (b).

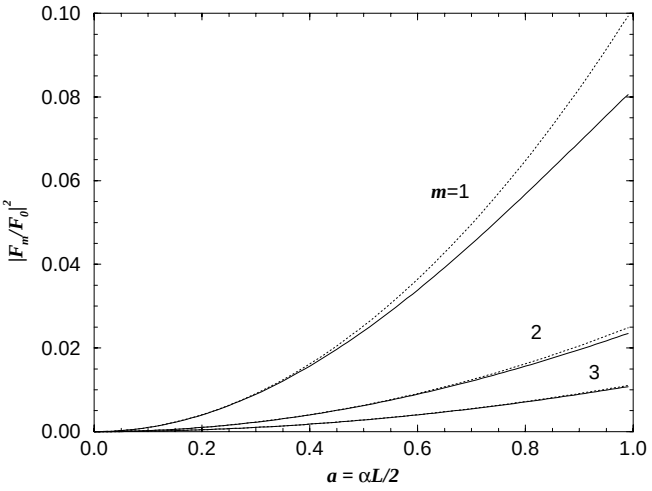

Figure 18. Calcualted values of $|F_m/F_0|^2$ as a function of a using the undepleted reference beam approximation (····) and numerical integration (—) for m = 1, 2, and 3.

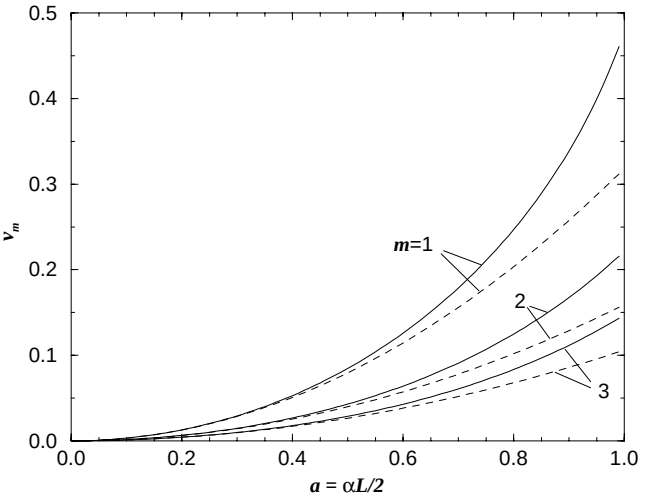

Figure 19. Calcualted values of v_m as a function of a using the undepleted reference beam approximation (····) and numerical integration (—) for m =1, 2, and 3.

$$NSR = \left| \sum_{m\neq 0} \frac{F_m}{F_0} \right|^2 = \left| \sum_{m\neq 0} \frac{a}{\pi m} e^{j\phi_m} \right|^2, \qquad (20)$$

where NSR denotes the crosstalk *noise-to-signal* ratio and ϕ_m is the phase of the m^{th} hologram (not to be confused with grating slant angle). The phase, ϕ_m, can be modeled as a random variable uniformly distributed between 0 and 2π, and it is assumed that each ϕ_m is mutually independent of each other. In this case, the expectation value of the expression on the right side of Eq. 20 is taken as the NSR:

$$\begin{aligned} NSR &= \left\langle \left| \sum_{m\neq 0} \frac{F_m}{F_0} \right|^2 \right\rangle \\ &= \sum_{m\neq 0} \sum_{m'\neq 0} \frac{a^2}{\pi^2 mm'} = \left\langle e^{j(\phi_m - \phi_{m'})} \right\rangle = \sum_{m'\neq 0} \left(\frac{a}{m} \right)^2 \\ &\leq 2 \sum_{m=1}^{\infty} \left(\frac{a}{m} \right)^2 = \frac{2}{3} a^2 = \frac{1}{6} (\alpha L)^2, \end{aligned} \qquad (21)$$

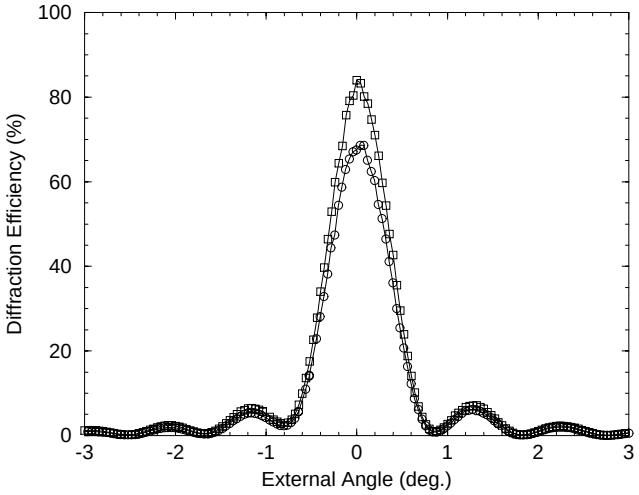

Figure 20. Angle selectivity profiles of $\Omega_{1_{ext}}$(□) and $\Omega_{2_{ext}}$(○) showing angular deviations, $\Delta\Omega_{1_{ext}}$ and $\Delta\Omega_{2_{ext}}$, from Bragg matching condition. The sample was pre-exposed with a fluence of 20 mJ/cm^2 at 514 nm, after which a non-slant holographic grating was recorded at 514 nm using a fluence of about 110 mJ/cm^2. The interbeam angle was 50°. The angle selectivity profile was obtained with an HeNe laser at 633 nm.

where $\sum_{m=1}^{\infty} 1/m^2 = \pi^2/6$, and $\left\langle e^{j(\phi_m - \phi_{m'})} \right\rangle = \delta_{mm'}$ (1, if $m = m'$; 0 otherwise).

Thus the upper limit of the crosstalk noise also scales quadratically with αL.

Note that from both experimental and theoretical results, the second null of the selectivity curve does not exhibit as much of an increase in diffraction efficiency as displayed by the first null. In an angular or wavelength multiplexed holographic storage system, adjacent holograms might therefore be written at the second null to reduce crosstalk. Since the crosstalk contribution scales quadratically with m, recording adjacent holograms at the second null reduces each crosstalk term in the summation of Eq. 21 by a factor of 4. Accordingly, the overall crosstalk noise, which occurs due to the deviation from an ideal sinc^2 Bragg selectivity profile, is also reduced by a factor of 4. The tradeoff, of course, is that the storage capacity is reduced by one half.

Conversely, if the dye concentration were fixed and the thickness L doubled, then although the angular separation of the nulls becomes halved, the amount of crosstalk would increase by a factor of 4. To achieve the same SNR thus requires that the angle separation be increased by a factor of 2. Accordingly, the same angle separation, and hence storage capacity, results as with a media of thickness L. Of course, the added thickness may provide for increased diffraction efficiency per hologram, but if sufficient dynamic range is obtained for thinner media, then no advantage exists in increasing the thickness as far as crosstalk noise is concerned. Lowering the dye concentration helps reduce the crosstalk noise, but the tradeoff is a diminution in sensitivity unless the other material components are altered or the composition is modified to provide for the necessary compensation.

In the analysis presented it was assumed that the average index of refraction is constant throughout the thickness of the recording medium. It should be mentioned that even in cases where n_1 is uniform, if n_0 varies with depth then changes also occur in the angular selectivity curve.[29]

The variation of n_0 in the photopolymer holographic recording material, ULSH-500, in the read state is negligible compared to the effect of non-uniform n_1, and thus the contribution of varying n_0 has been ignored in the above analysis. It was assumed, however, that n_1 decays exponentially with z. Since it was also assumed that αL is small and

$$e^{-\alpha z} \approx 1 - \alpha z, \tag{22}$$

then the case studied is actually similar to a small linear perturbation. The results presented herein should then fit many situations adequately, provided the perturbation in n_1 is small and dominantly linear in z. This condition will exist if the absorbance of the recording medium is sufficiently low.

It has been observed that cases exist where the experimental results cannot be explained by the simple exponentially decaying n_1 model. This is likely due to a more complicated dependency of n_1 on z. In theory n_1 could be deduced from the angular selectivity curve. Unfortunately, even where the undepleted reference beam approximation is applicable, only the amplitude of the Fourier transform of n_1 is measured, and not the phase, and thus an inverse Fourier transform cannot be carried out to obtain the functional dependence of n_1.

Conclusion

A new photopolymer holographic recording material ULSH-500 based on cationic ring-opening polymerization has been further optimized to achieve low transverse shrinkage without sacrificing sensitivity or dynamic range. The magnitude of the shrinkage in the transverse direction was diminished to acceptably low levels for angle multiplexing holograms of low diffraction efficiency, by carrying out a low-level pre-imaging exposure. Moreover, angular selectivity profiles exhibited the expected sinc^2 function behavior with minimal background uplift, and good image uniformity was observed. A pre-imaging exposure fluence, between 30 and 40 mJ/cm^2, was sufficient to reduce the magnitude of the angular deviations from the Bragg matching condition to $\leq 0.1°$, even for holograms with diffraction efficiency of less than 0.1% and grating slant angle of $\phi = 20°$. The extent of transverse (z) and lateral (x) shrinkage was determined explicitly in this study for a range of grating slant angles, in volume holograms recorded to near saturation, and in holograms of low diffraction efficiency. $\Delta K_x/K_x$ and $\Delta K_z/K_z$, which represent the physical material shrinkage in the grating vector plane, were ascertained without assuming that anchoring exists at the substrate interface. The Dual Differential Angle Measurement (DDAM) method implemented comprised (1) direct measurement of the differential angle changes in the reference and signal beam angles necessary to achieve Bragg matching and (2) measurement of the average refractive index. The assumption of anchoring and thus uniaxial shrinkage, as embodied in the conventional fringe rotation model, cannot be applied for the photopolymer ULSH-500 under the recording conditions described. When the change in refractive index during hologram formation is is taken into account, then the assumption of anchorage more closely applies, and a reduction in the overestimation of shrinkage results. The first order approximation solution for the DDAM method deviates from the exact solution result for cases of large grating slant angles.

Uplifts in the angle selectivity curve were observed in certain cases, which can be attributed to a non-uniform grating strength throughout the thickness of the recording medium. This originates from the decrease in light intensity due to absorbance and the concomitant decrease in grating strength, as light transmits through the recording medium. According to the model presented herein, if the dye concentration in the recording medium is fixed and the thickness L is doubled, then although the angular separation of the nulls is halved, the amount of crosstalk that results increases by a factor of 4. To achieve the same SNR thus requires that the angle separation be increased by a factor of 2, and therefore the identical angle separation, and hence storage capacity, results as with a media of thickness L. Although the added thickness may provide for increased diffraction efficiency per hologram, no advantage is realized for this type of crosstalk noise when the thickness is increased. Lowering the dye concentration helps reduce this crosstalk noise, but the tradeoff is sensitivity is diminished unless other material components are altered or the composition modified to provide for necessary compensation.

Acknowledgment. We thank P. K. Dhal for his assistance in synthesis and R. T. Ingwall for his assistance in purification and for helpful discussions.

References

1. D. A. Waldman, R. T. Ingwall, P. K. Dhal, M. G. Horner, E. S. Kolb, H.-Y. S. Li, R. A. Minns, and H. G. Schild, Cationic ring-opening photopolymerization methods for volume hologram recording, *Diffractive and Holographic Optics Technology III*, Proc. SPIE **2689,** 15, 127 (1996).
2. R. K. Sadhir and R. M. Luck, *Expanding Monomers*, CRC Press, Boca Raton, 1992, Chapter 1.
3. U.-S. Rhee, H. J. Caulfield, C. S. Vikram, and J. Shamir, Dynamics of hologram recording in DuPont photopolymer, *Appl. Opt.* **34** (5), 846 (1995).
4. M. Ono, M. Uchida, A. Masui, N. Nakazawa, H. Sakurai, and M. Hirano, IDT-SEM observation of fringe pattern in volume hologram and its appplication to multicolor recorded HOEs, *Proc. SPIE* **3011**, 24 (1997).
5. (a) F. M. Smits and L. E. Gallagher, Design considerations for a semipermanent optical memory, *Bell. Syst. Tech. J.* **46,** 1267 (1967); (b) C. B. Burckhardt and E. T. Doherty, *Appl. Opt.* **8,** 2479 (1969).
6. (a) L. d'Auria, J. P. Huignard, C. Slezak, and E. Spitz, Experimental holographic read-write memory using 3-D storage, *Appl. Opt.* **13** (4), 808 (1974); (b) F. H. Mok, Angle-multiplexed storage of 5000 holograms in lithium niobate, *Opt. Lett.* **18** (11), 915 (1993).
7. C. B. Burckhardt, Use of a random phase mask for the recording of Fourier transform holograms of data masks, *Appl. Opt.* **9** (3), 695 (1970).
8. A. A. Verbovetskii and V. B. Fedorov, Recording of binary data in paraphase code on phase holograms, *Opt. Spektrosk.* **33** (1), 628 (1972).
9. H. J. Caulfield, Spatially randomized data masks for holographic storage, *Appl. Opt.* **9,** 2587 (1970).
10. A. A. Verbovetskii, A. P. Grammatin, V. N. Ivanov, V. G. Mityakov, A. A. Novikov, N. N. Rukavitsin, Yu. S. Skvortsov, V. B. Fedorov, and V. V. Tsvetkov, Holographic memory for archival storage of binary information, *Sov. J. Opt. Technol.* **55** (5), 280 (1988).
11. M. A. Neifeld and M. McDonald, Error correction for increasing the usable capacity of photorefractive memories,*Opt. Lett.* **19** (18), 1483 (1994).
12. J. F. Heanue, M. C. Bashaw, and L. Hesselink, Channel codes for digital holographic data storage, *J. Opt. Soc. Am. A*, **12** (11), 2432 (1995).
13. L. Solymer and D. J. Cooke, Volume holography and volume gratings, Academic Press, New York, 1981.
14. J. V. Crivello and J. L. Lee, Alkoxy-substituted diaryliodonium salt cationic photoinitiators, *J. Poly. Sci., Part A: Polym. Chem. Ed.* **27**, 3951 (1989).
15. D. H. R. Vilkomerson and D. Bostwick, Some effects of emulsion shrinkage on a hologram's image space, *Appl. Opt.*, **6** (7), 1270 (1967).
16. J. T. Gallo and C. M. Verber, Model for the effects of material shrinkage on volume holograms, *Appl. Opt.*, **33** (29), 6797 (1994).
17. F. Lohse and H. Zweifel, Photocrosslinking of epoxy resins, *Adv. Poly. Sci.* **78**, 62 (1986).
18. R. P. Eckberg, *Radiation Curing in Polymer Science and Technol.*, J. P. Fovassier and J. F. Rabek, Eds., Elsevier, London, 1993, Vol. IV, Ch. 2, pp. 19-50.
19. A. Pu, K. Curtis, and D. Psaltis, Exposure schedule for multiplexing

holograms in photopolymer films, *Opt. Eng.* **35** (10), 2824 (1996).
20. H. Kogelnik, Coupled wave theory for thick hologram gratings, *Bell Syst. Tech. J.* **48,** 2909 (1969).
21. N. Uchida, Calculation of diffraction efficiency in hologram gratings attenuated along the direction perpendicular to the grating vector, *J. Opt. Soc. Am.* **63,** 280 (1973).
22. R. Kowarschik, Diffraction efficiency of attenuated sinusoidally modulated gratings in volume holograms, *Opt. Acta* **23,** 1039 (1976).
23. S. Morozumi, Diffraction efficiency of hologram gratings with modulation changing through the thickness, *Jp. J. Appl. Phys.* **15**, 1929 (1976).
24. T. Kubota, Characteristics of thick hologram gratings recorded in absorptive medium, *Opt. Acta* **25**, 1035 (1978).
25. U. Killat, Coupled wave theory of hologram gratings with arbitrary attenuation, *Opt. Comm.* **21**, 110 (1977).
26. F. Lederer and U. Langbein, Attenuated thick hologram gratings, Part I, Diffraction efficiency, *Opt. Quant. Electron.* **9,** 473 (1977).
27. F. Lederer and U. Langbein, Attenuated thick hologram gratings, Part II, Anomalous absorption, *Opt. Quant. Electron.* **9**, 487 (1977).
28. T. Kubota, The diffraction efficiency of hologram gratings recorded in an absorptive medium, *Opt. Comm.* **16**, 347 (1976).
29. M. P. Owen and L. Solymar, Efficiency of volume phase reflection holograms recorded in an attenuated medium, *Opt. Comm.* **34**, 321 (1980).
30. D. Brady, K. Hsu, and D. Psaltis, Periodically Refreshed Multiply Exposed Photorefractive Holograms, *Opt. Lett.,* **15** (14), 817 (1990).
31. Details of calculation to be published.
32. C. Gu, J. Hong, I. McMichael, R. Saxena, and F. Mok, Cross-talk-limited storage capacity of volume holographic memory, *J. Opt. Soc. Am. A* **9** (11), 1 (1992).
33. K. Curtis, D. Psaltis, and C. Gu, Crosstalk in wavelength multiplexed holographic memories, *Opt. Lett.* **18** (12), 1001 (1993).